

---

# TEMPORALLY UNIFIED ADVERSARIAL PERTURBATIONS FOR TIME SERIES FORECASTING

---

**Ruixian Su**

School of Management

Huazhong University of Science and Technology  
ruixiansu@hust.edu.cn

**Yukun Bao**

School of Management

Huazhong University of Science and Technology  
yukunbao@hust.edu.cn

**Xinze Zhang\***

School of Computer Science and Technology

Huazhong University of Science and Technology  
xinze@hust.edu.cn

February 13, 2026

## ABSTRACT

While deep learning models have achieved remarkable success in time series forecasting, their vulnerability to adversarial examples remains a critical security concern. However, existing attack methods in the forecasting field typically ignore the temporal consistency inherent in time series data, leading to divergent and contradictory perturbation values for the same timestamp across overlapping samples. This temporally inconsistent perturbations problem renders adversarial attacks impractical for real-world data manipulation. To address this, we introduce Temporally Unified Adversarial Perturbations (TUAPs), which enforce a temporal unification constraint to ensure identical perturbations for each timestamp across all overlapping samples. Moreover, we propose a novel Timestamp-wise Gradient Accumulation Method (TGAM) that provides a modular and efficient approach to effectively generate TUAPs by aggregating local gradient information from overlapping samples. By integrating TGAM with momentum-based attack algorithms, we ensure strict temporal consistency while fully utilizing series-level gradient information to explore the adversarial perturbation space. Comprehensive experiments on three benchmark datasets and four representative state-of-the-art models demonstrate that our proposed method significantly outperforms baselines in both white-box and black-box transfer attack scenarios under TUAP constraints. Moreover, our method also exhibits superior transfer attack performance even without TUAP constraints, demonstrating its effectiveness and superiority in generating adversarial perturbations for time series forecasting models.

**Keywords** Time Series Forecasting, Adversarial Attack, Temporally Unified Adversarial Perturbation, Timestamp-wise Gradient Accumulation Method

## 1 Introduction

Deep-learning-based time series forecasting has been widely deployed due to its superior predictive performance, serving as a pivotal tool for operations and risk management across critical sectors, such as smart grids [1], manufacturing [2], and finance [3]. Despite these advances, recent studies have revealed that deep learning models are vulnerable to adversarial examples, *i.e.*, inputs with carefully crafted perturbations that lead to incorrect predictions [4]. This particularly indicates the adversarial vulnerability in time series forecasting applications, where malicious perturbations could mislead forecasting systems into making erroneous decisions with catastrophic consequences. Consequently,

---

\*Corresponding author: Xinze Zhang.

investigating the reliability and robustness of time series forecasting models under adversarial attacks has garnered considerable attention.

While adversarial attacks in vision and language domains have been extensively studied, attacks in the forecasting field remain limited. Early attempts at adversarial attacks on time series forecasting directly adapted image-based attack methods, such as the Fast Gradient Sign Method (FGSM) [5], treating time series as one-dimensional images [6, 7]. However, such adaptations neglect the unique temporal dependencies in time series [8]. More recent works have begun to tailor adversarial attack strategies specifically for time series forecasting, such as the importance measuring method AAIM [9], the temporal similarity constraint method TCA [10], and the attack direction selection method AAJM [11], which have significantly enhanced the effectiveness of adversarial attacks in the time series forecasting domain.

Despite their efficacy, existing methods overlook the auto-regressive sliding-window characteristic of time series forecasting, which makes forecasting tasks inherently distinct from other tasks. This mechanism implies that a historical value at a specific timestamp is repeatedly sampled and observed within multiple input samples. Since conventional attack frameworks optimize perturbations for each sample in isolation, they inevitably generate divergent, often contradictory, perturbation values for the same timestamp across different samples, leading to the "temporally inconsistent perturbations" problem. This lack of temporal consistency renders such adversarial examples impractical for real-world data manipulation, thereby hindering a realistic evaluation of the adversarial robustness of time series forecasting systems.

To address these limitations, we propose a novel and practical concept of adversarial perturbations, namely Temporally Unified Adversarial Perturbations (TUAPs), which significantly degrade the accuracy of state-of-the-art forecasting models while explicitly enforcing a temporal unification constraint that ensures the perturbation at each specific timestamp is shared across all overlapping samples. Since TUAPs impose a more stringent constraint on the perturbation space, generating effective TUAPs is more challenging than crafting traditional perturbations. To effectively generate TUAPs, we further propose a modular and efficient Timestamp-wise Gradient Accumulation Method (TGAM), by aggregating local gradient information from overlapping samples to optimize perturbations under the temporal consistency constraint. Through integrating TGAM with momentum-based attack algorithms, we demonstrate that our proposed method can be easily incorporated into existing attack frameworks to enhance their effectiveness for time series forecasting. Our main contributions are summarized as follows:

- We pioneer the investigation of Temporally Unified Adversarial Perturbations (TUAPs) for time series forecasting, demonstrating that state-of-the-art forecasting models can be effectively attacked across all overlapping samples using temporally unified perturbations that maintain practical feasibility.
- We propose the Timestamp-wise Gradient Accumulation Method (TGAM) to effectively generate TUAPs, which efficiently aggregates gradient information from overlapping samples to optimize perturbations under the temporal consistency constraint.
- We conduct extensive experiments demonstrating that our proposed method significantly outperforms all baselines in both white-box and black-box attack scenarios under TUAP constraints, and even exceeds unconstrained baselines in transfer attack scenarios, demonstrating its effectiveness and superiority in attacking time series forecasting models.

The remainder of this paper is organized as follows. Section 2 provides preliminaries on time series forecasting and reviews related work on adversarial attacks. Section 3 details the motivation of this work, the definition of TUAPs, and the implementation of our proposed TGAM. Section 4 presents the experimental setup, results, and analysis. Finally, Section 5 concludes the paper and discusses future research.

## 2 Related Work

### 2.1 Preliminaries

As shown in Fig. 1, in a general time series forecasting task, the objective is to predict a sequence of future observations based on a given sequence of historical data. Typically, consider a raw time series  $\mathcal{V} = \{\mathbf{v}_1, \mathbf{v}_2, \dots, \mathbf{v}_t, \dots, \mathbf{v}_T\} \in \mathbb{R}^{T \times D}$ , where  $T$  is the total length of the time series,  $\mathbf{v}_t \in \mathbb{R}^D$ ,  $\mathbf{v}_t = [v_t^1, v_t^2, \dots, v_t^D]$  denotes the observation vector at time  $t$ , and  $D$  is the dimension (number of variables) of each observation. Forecasting models employ a sliding-window mechanism to consecutively sample  $\mathcal{V}$  without strides<sup>2</sup> to construct a time series dataset  $\mathcal{D}$  that consists of  $N$  input-target pairs  $\{(\mathbf{x}_n, \mathbf{y}_n)\}_{n=1}^N$ .

<sup>2</sup>We provide a dynamical visualization of what this non-stride sampling does in the link: [https://github.com/Simonnop/time\\_series\\_sampling/blob/main/README.md](https://github.com/Simonnop/time_series_sampling/blob/main/README.md)

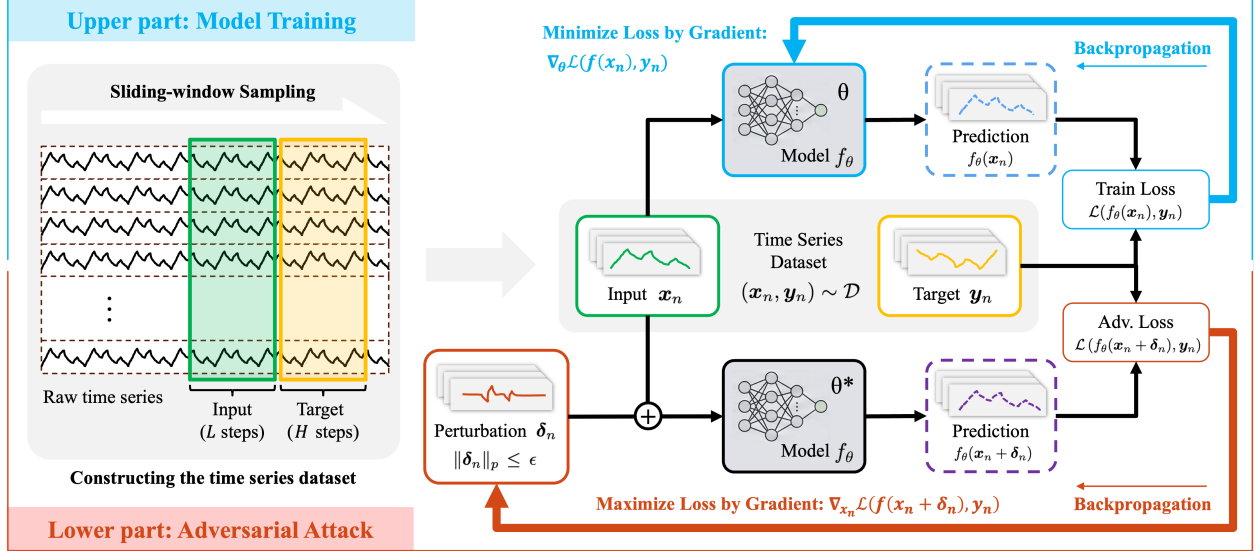


Figure 1: Illustration of the preliminaries of time series forecasting and adversarial attack on time series forecasting.

Specifically, let  $L$  denote the input lookback window length and  $H$  denote the forecasting horizon. The input  $\mathbf{x}_n \in \mathbb{R}^{L \times D}$  and target  $\mathbf{y}_n \in \mathbb{R}^{H \times D}$  are sampled as  $\mathbf{x}_n = [\mathbf{v}_n, \mathbf{v}_{n+1}, \dots, \mathbf{v}_{n+L-1}]$  and  $\mathbf{y}_n = [\mathbf{v}_{n+L}, \mathbf{v}_{n+L+1}, \dots, \mathbf{v}_{n+L+H-1}]$ , respectively. For brevity, let  $\mathbf{v}_{n:n+L-1} = [\mathbf{v}_n, \mathbf{v}_{n+1}, \dots, \mathbf{v}_{n+L-1}]$  denote the time series values from timestamp  $n$  to timestamp  $n+L-1$ , so that  $\mathbf{x}_n = \mathbf{v}_{n:n+L-1}$ ,  $\mathbf{y}_n = \mathbf{v}_{n+L:n+L+H-1}$ , and  $N = T - L - H + 1$ .

Deep forecasting models learn a mapping function  $f_\theta : \mathcal{X} \rightarrow \mathcal{Y}$ , where  $\mathcal{X} \subseteq \mathbb{R}^{L \times D}$  and  $\mathcal{Y} \subseteq \mathbb{R}^{H \times D}$  are the input and target spaces, respectively. The objective is to minimize a loss function  $\mathcal{L}(\cdot, \cdot)$  (e.g., mean squared error [12, 13]) between the prediction  $\hat{\mathbf{y}}_n = f_\theta(\mathbf{x}_n)$  and the ground truth  $\mathbf{y}_n$  with the optimal parameters  $\theta^*$ :

$$\theta^* = \underset{\theta}{\operatorname{argmin}} \mathcal{L}(\hat{\mathbf{y}}_n, \mathbf{y}_n). \quad (1)$$

In contrast, adversarial attacks aim to find an adversarial example  $\mathbf{x}'_n = \mathbf{x}_n + \delta_n$  within a small neighborhood of the original input  $\mathbf{x}_n$  that causes erroneous predictions, where  $\delta_n$  is the adversarial perturbation. For each sample  $\mathbf{x}_n$ , the objective is to maximize the loss function  $\mathcal{L}(\cdot, \cdot)$  between the prediction  $\hat{\mathbf{y}}'_n = f_\theta(\mathbf{x}'_n)$  and the ground truth  $\mathbf{y}_n$  with the optimal perturbation  $\delta_n^*$ :

$$\delta_n^* = \underset{\delta_n}{\operatorname{argmax}} \mathcal{L}(\hat{\mathbf{y}}'_n, \mathbf{y}_n) \quad \text{s.t.} \quad \|\delta_n\|_p \leq \epsilon, \quad (2)$$

where  $\|\delta_n\|_p \leq \epsilon$  constrains the perturbation magnitude, *i.e.*, the  $L_p$  norm of the perturbation  $\delta_n$  must be less than or equal to a threshold  $\epsilon$ , with  $L_\infty$  being the most commonly adopted norm [14, 15].

## 2.2 Foundational Adversarial Attack Methods

Adversarial attacks serve as an important tool for assessing the adversarial robustness of deep learning models. Since Szegedy et al. [4] first identified the vulnerability of Deep Neural Networks (DNNs), research in this field has flourished, primarily within the computer vision domain. As a foundational work, Goodfellow et al. [5] propose the Fast Gradient Sign Method (FGSM), which generates adversarial perturbations via a single-step update along the direction of the loss gradient:

$$\delta_n = \epsilon \cdot \operatorname{sign}(\nabla_{\mathbf{x}_n} \mathcal{L}(\hat{\mathbf{y}}_n, \mathbf{y}_n)) = \begin{cases} \epsilon, & \text{if } \nabla_{\mathbf{x}_n} \mathcal{L}(\hat{\mathbf{y}}_n, \mathbf{y}_n) > 0 \\ 0, & \text{if } \nabla_{\mathbf{x}_n} \mathcal{L}(\hat{\mathbf{y}}_n, \mathbf{y}_n) = 0 \\ -\epsilon, & \text{if } \nabla_{\mathbf{x}_n} \mathcal{L}(\hat{\mathbf{y}}_n, \mathbf{y}_n) < 0 \end{cases} \quad (3)$$

where  $\operatorname{sign}(\cdot)$  is the sign function, and  $\nabla_{\mathbf{x}_n} \mathcal{L}(\hat{\mathbf{y}}_n, \mathbf{y}_n)$  is the gradient of the loss  $\mathcal{L}(\hat{\mathbf{y}}_n, \mathbf{y}_n)$  with respect to  $\mathbf{x}_n$ . While efficient, this single-step attack may be limited in effectiveness on complex model architectures due to its simplistic optimization of adversarial perturbations.

To overcome the limitations of FGSM, Kurakin et al. [16] propose an iterative variant known as the Basic Iterative Method (BIM). Let  $k \in \{0, 1, \dots, K-1\}$  denote the iteration index and  $K$  denote the maximum number of iterations.

$\mathbf{x}'_n^k$  and  $\delta_n^k$  denote the adversarial example and adversarial perturbation at the  $k$ -th iteration, BIM can be formulated as:

$$\mathbf{x}'_n^{k+1} = \mathbf{x}_n + \delta_n^{k+1}, \quad (4)$$

$$\delta_n^{k+1} = \text{clip}(\tilde{\delta}_n^{k+1}, \epsilon) = \begin{cases} \epsilon, & \text{if } \tilde{\delta}_n^{k+1} > \epsilon, \\ -\epsilon, & \text{if } \tilde{\delta}_n^{k+1} < -\epsilon, \\ \tilde{\delta}_n^{k+1}, & \text{otherwise,} \end{cases} \quad (5)$$

$$\tilde{\delta}_n^{k+1} = \delta_n^k + \alpha \cdot \text{sign}(\nabla_{\mathbf{x}'_n^k} \mathcal{L}(f_\theta(\mathbf{x}'_n^k), \mathbf{y}_n)), \quad (6)$$

where  $\mathbf{x}'_n^0 = \mathbf{x}_n$ ,  $\delta_n^0 = \mathbf{0}$ , and  $\alpha$  is the step size with  $\alpha < \epsilon$ . This iterative approach allows for a more thorough exploration of the adversarial space. Facing the issue of getting trapped in local extrema during optimization, Madry et al. [17] propose Projected Gradient Descent (PGD), which extends BIM by introducing random initialization. By starting from a random point within the  $\epsilon$ -neighborhood, such as  $\mathbf{x}'_n^0 = \mathbf{x}_n + \text{Uniform}(-\epsilon, \epsilon)$ , PGD provides a stronger and more reliable attack than BIM.

Furthermore, to improve the transferability of adversarial examples, Dong et al. [18] propose Momentum Iterative FGSM (MI-FGSM) by integrating a momentum term into the iterative update of BIM, which stabilizes the update direction and helps escape poor local maxima:

$$\tilde{\delta}_n^{k+1} = \delta_n^k + \alpha \cdot \text{sign}(\mathbf{m}_n^k), \quad (7)$$

$$\mathbf{m}_n^{k+1} = \mu \cdot \mathbf{m}_n^k + \frac{\nabla_{\mathbf{x}'_n^k} \mathcal{L}(f_\theta(\mathbf{x}'_n^k), \mathbf{y}_n)}{\|\nabla_{\mathbf{x}'_n^k} \mathcal{L}(f_\theta(\mathbf{x}'_n^k), \mathbf{y}_n)\|_1}, \quad (8)$$

where  $\mathbf{m}_n^k$  is the accumulated momentum term at  $k$ -th iteration,  $\mathbf{m}_n^0 = \mathbf{0}$ , and  $\mu$  is the decay factor.

Building on these classical methods, numerous variants have been proposed focusing on gradient refinement [19, 20], ensemble surrogate models [21], and input transformation techniques [22, 23], leading to enhanced attack effectiveness in white-box settings and improved adversarial transferability in black-box settings. While these methods provide a solid technical foundation for adversarial attacks, they are primarily designed for image-based tasks and do not explicitly account for the unique characteristics of time series forecasting.

### 2.3 Adversarial Attacks for Time Series Forecasting

Compared to the extensive research on adversarial attacks in the image domain, studies focusing on time series forecasting tasks have emerged more recently and remain relatively limited.

Initially, the primary approach was to adapt well-established adversarial attack techniques directly from the image domain to time series models by replacing the input  $\mathbf{x}_n$  (from images to time series) and the loss function  $\mathcal{L}$  (from Cross-Entropy classification loss to Mean Squared Error regression loss):

$$\mathcal{L}(\hat{\mathbf{y}}'_n, \mathbf{y}_n) = \frac{1}{H} \sum_{h=1}^H (\hat{\mathbf{y}}'_{n,h} - \mathbf{y}_{n,h})^2, \quad (9)$$

where  $\mathbf{y}_{n,h} = \mathbf{v}_{n+L+h-1}$  and  $\hat{\mathbf{y}}'_{n,h}$  are the ground-truth and prediction values at the  $h$ -th horizon step of  $\mathbf{y}'_n$ , respectively. Following this approach, Mode and Hoque [6] transfer FGSM and BIM to craft adversarial multivariate time series examples for CNN, LSTM, and GRU, demonstrating that adversarial examples exhibit effectiveness and transferability in time series forecasting. Similarly, Heinrich et al. [7] utilize PGD to construct adversarial examples for CNN and LSTM in wind power forecasting tasks. In addition to gradient-based methods, Wang et al. [24] formulate the generation of adversarial perturbations as a discrete optimization problem and utilize Bayesian Optimization (BO) to explore perturbations on CNN, LSTM, and Attention-based TCN. These investigations highlight the vulnerability of deep learning models in time series forecasting domains.

Beyond directly applying existing methods, researchers have made efforts to improve these classical methods to better suit the forecasting domain, primarily focusing on preserving the imperceptibility of adversarial attacks in time series. A natural approach is to selectively perform adversarial attacks on different time steps. Wu et al. [9] propose the Adversarial Time Series Generator (ATSG), which is based on FGSM but replaces the MSE loss in Eq. (9) with a Mean Absolute Error (MAE) function:

$$\mathcal{L}_{\text{ATSG}} = \frac{1}{H} \sum_{h=1}^H |\hat{\mathbf{y}}'_{n,h} - \mathbf{y}_{n,h}|. \quad (10)$$

The authors [9] further proposed the Adversarial Attack with Importance Measuring (AAIM), which selectively applies perturbations to critical time steps within each input sample. AAIM first generates candidate perturbations  $\delta_n$  with ATSG, then calculates importance scores for each time step using a masking operation similar to textual adversarial attacks [25, 26], and finally retains perturbations only on the most important time steps while resetting others to their benign values, thereby improving attack imperceptibility.

Considering selective adversarial attacks on different input samples, Jiao et al. [11] propose a sample selection method and an Attack Direction Judgment Method (ADJM). Specifically, the authors train a binary Support Vector Machine (SVM) to perform sample selection, determining whether each sample should be perturbed. Then, ADJM employs FGSM with the objective of maximizing or minimizing the forecasting value:

$$\mathcal{L}_{\text{ADJM}} = \lambda_n \cdot \hat{y}'_{n,h}, \quad (11)$$

where  $\lambda_n \in \{1, -1\}$  denotes the attack direction and is predicted via another binary SVM for each selected sample  $x_n$ .

Besides selective adversarial attacks, similarity between adversarial and benign samples has been considered to constrain perturbations. Shen and Li [10] propose Temporal Characteristics-based Attack (TCA) by modifying the numerical comparison in BIM’s clip operation with cosine similarity comparison, replacing  $\text{clip}(\cdot, \epsilon)$  in Eq. (5) as:

$$\text{clip}_{\text{TCA}}(\tilde{\delta}_n^k, \epsilon) = \begin{cases} \epsilon, & \text{if } \text{sim}(x_n, x_n + \epsilon) > \max(\text{sim}(x_n, x_n - \epsilon), \text{sim}(x_n, x_n + \tilde{\delta}_n^k)), \\ -\epsilon, & \text{if } \text{sim}(x_n, x_n - \epsilon) > \max(\text{sim}(x_n, x_n + \epsilon), \text{sim}(x_n, x_n + \tilde{\delta}_n^k)), \\ \tilde{\delta}_n^k, & \text{otherwise,} \end{cases} \quad (12)$$

where  $\text{sim}(\cdot, \cdot)$  is the cosine similarity function. Through this operation, TCA effectively crafts perturbed samples  $x'_n$  that maintain higher similarity to the original samples  $x_n$  than previous attack methods.

Despite these efforts, existing adversarial attack methods for time series forecasting still follow the sample-independent attack paradigm derived from the image domain, generating perturbations independently for each input sample. Although imperceptibility is improved by selectively attacking critical time steps within each sample or by constraining similarity between adversarial and benign samples, these works all focus on sample-level imperceptibility. This is analogous to adversarial attacks on images that tolerate pixel-level noise invisible to human perception independently for each image, but it neglects the intrinsic temporal consistency requirement across consecutive samples in time series data. Specifically, due to the sliding-window mechanism in time series forecasting, the same timestamp appears in multiple overlapping samples, yet existing methods may assign contradictory perturbation values to the same timestamp across different samples, making such attacks physically unrealizable in real-world data manipulation scenarios. Therefore, this study addresses this critical limitation by introducing temporally unified adversarial perturbations that ensure consistency across all overlapping samples.

### 3 Methodology

In this section, we detail the definition and generation of Temporally Unified Adversarial Perturbations (TUAPs). We begin by discussing the core motivations behind TUAPs, specifically addressing the temporally inconsistent perturbations issue caused by existing adversarial attacks in the forecasting domain. Next, we provide a formal definition of TUAPs, introducing a constraint for temporal consistency across overlapping samples. Then, with the updated adversarial objective, we introduce the Timestamp-wise Gradient Sign Method (TGSM) and the Timestamp-wise Gradient Accumulation Method (TGAM) to effectively generate TUAPs. Finally, we present MI-TGAM as our final implementation, which incorporates a momentum-based update mechanism to enhance attack effectiveness and transferability.

#### 3.1 Motivation

In the field of time series forecasting, adversarial attacks must account for temporal consistency across consecutive samples to remain practically imperceptible. Under the sliding-window sampling mechanism, which is the fundamental principle for segmenting the raw time series to construct datasets, an observed value at a specific timestamp is shared across multiple overlapping samples. However, existing adversarial attack methods generate different adversarial perturbations for the same timestamp across overlapping samples. This leads to a crucial problem that we refer to as “temporally inconsistent perturbations”, making it impossible to assign a unique perturbation to a specific timestamp in reality.

Specifically, consider two adjacent input samples  $x_n$  and  $x_{n+1}$  derived from the raw time series  $\mathcal{V} = \{v_1, v_2, \dots, v_T\}$ , where  $x_n = v_{n:n+L-1}$  and  $x_{n+1} = v_{n+1:n+L}$  share the overlapping segment  $v_{n+1:n+L-1}$ . When generating

adversarial examples with existing methods, since the loss function values for  $\mathbf{x}_n$  and  $\mathbf{x}_{n+1}$  are different as  $\mathcal{L}(\hat{\mathbf{y}}_n, \mathbf{y}_n) \neq \mathcal{L}(\hat{\mathbf{y}}_{n+1}, \mathbf{y}_{n+1})$ , leading to inconsistent gradients as  $\nabla_{\mathbf{x}_n} \mathcal{L}(\hat{\mathbf{y}}_n, \mathbf{y}_n) \neq \nabla_{\mathbf{x}_{n+1}} \mathcal{L}(\hat{\mathbf{y}}_{n+1}, \mathbf{y}_{n+1})$ . Even though some gradient components may be clipped to the same magnitude  $\epsilon$ , this still leads to an extremely high probability of producing divergent perturbations for the shared timestamps.

This violates an important and natural constraint in the time series forecasting domain: once a timestamp is observed, its value becomes part of the fixed historical record and cannot be changed retroactively. Since the observations  $\mathbf{v}_{n+1:n+L-1}$  are historical and shared between both samples, once perturbations are applied to these timestamps, they become part of the fixed history and must be identical in both samples to maintain temporal consistency. In contradiction to this requirement, existing adversarial attack methods generate inconsistent perturbations for the same timestamp, resulting in  $\delta_{n,l+1} \neq \delta_{n+1,l}$ , where  $\delta_{n,l}$  denotes the generated adversarial perturbation for sample  $\mathbf{x}_n$  at the  $l$ -th time step. This temporally inconsistent perturbations problem poses several practical challenges when imposing adversarial perturbations on the input time series, such as the need for repeated perturbation injection for the same timestamp (which can be easily detected), and the same-timestamp adversarial perturbation selection problem (which remains unexplored).

To address the temporally inconsistent perturbations problem, we formally define Temporally Unified Adversarial Perturbations (TUAPs), which extend the adversarial attack scope from individual time series samples to the entire time series. We then introduce the Timestamp-wise Gradient Sign Method (TGSM), which provides a straightforward approach for generating TUAPs. Additionally, to further enhance computational efficiency and attack effectiveness, we develop the Timestamp-wise Gradient Accumulation Method (TGAM), which provides a modular framework to improve attack performance. Finally, we present MI-TGAM as our final implementation, which embeds the momentum-based update mechanism of MI-FGSM into TGAM to further enhance attack effectiveness and transferability.

### 3.2 Temporally Unified Adversarial Perturbation

To better highlight the difference between our proposed temporally unified adversarial perturbations and existing adversarial perturbations, we first formally summarize previous works and provide their conception of time series forecasting adversarial perturbations as follows.

**Definition 1 (Adversarial Perturbation)** *Given a subset of (test) time series samples  $\mathcal{S} \in \mathcal{D}$  and a small constant  $\epsilon > 0$ , an adversarial perturbation is an additive noise in the adversarial perturbation space*

$$\mathcal{A} = \{\delta \mid \exists (\mathbf{x}, \mathbf{y}) \in \mathcal{S}, \|\delta\|_\infty \leq \epsilon \wedge \ell(f_\theta(\mathbf{x}), \mathbf{y}) \leq \xi \wedge \ell(f_\theta(\mathbf{x} + \delta), \mathbf{y}) > \gamma\}, \quad (13)$$

*which consists of all possible perturbations  $\delta$  that fool the forecasting model  $f_\theta(\cdot)$  on  $\mathbf{x} + \delta$ , where  $\ell(\cdot, \cdot)$  is a metric for evaluating forecasting error, and  $\xi \leq \gamma$  are thresholds for acceptable and unacceptable forecasting quality, respectively.*

The constraint  $\ell(f_\theta(\mathbf{x}), \mathbf{y}) \leq \xi \wedge \ell(f_\theta(\mathbf{x} + \delta), \mathbf{y}) > \gamma$  ensures that the forecasting model is reliable on clean data  $\mathbf{x}$  but vulnerable to the adversarial example  $\mathbf{x} + \delta$ . In practice,  $\ell(f_\theta(\mathbf{x}), \mathbf{y}) \leq \xi$  and  $\ell(f_\theta(\mathbf{x} + \delta), \mathbf{y}) > \gamma$  are achieved by performing the optimization as shown in Eq. (1) and Eq. (2), respectively.

While Definition 1 is reasonable for individual samples in conventional settings, where an adversary typically seeks an optimal perturbation  $\delta_n$  to maximize the forecasting error for each sample  $\mathbf{x}_n$  independently, we argue that generating adversarial perturbations for multiple samples without considering temporal unification is inappropriate in time series forecasting, because the same timestamp shared by multiple samples should be perturbed identically to maintain temporal coherence.

Building upon the motivation discussed above, we formally define temporally unified adversarial perturbations for time series forecasting, which ensure that the perturbation applied to the same timestamp is shared across all overlapping samples.

**Definition 2 (Temporally Unified Adversarial Perturbations)** *Within Definition 1, a temporally unified adversarial perturbation is an additive noise in the adversarial perturbation space*

$$\mathcal{U} = \{\delta_n \in \mathcal{A} \mid \forall \mathbf{v}_t = \mathbf{x}_{n,l} = \mathbf{x}_{i,j}, \delta_{n,l} = \delta_{i,j} = \mathbf{p}_t \wedge \forall p_t^d \in \mathbf{p}_t, |p_t^d| \leq \epsilon \cdot |v_t^d|\}, \quad (14)$$

*where  $\mathbf{v}_t = \mathbf{x}_{n,l} = \mathbf{x}_{i,j}$  denotes that input samples  $\mathbf{x}_n$  and  $\mathbf{x}_i$  overlap at the historical value  $\mathbf{v}_t$  at timestamp  $t$  (i.e.,  $\mathbf{x}_{n,l} = \mathbf{x}_{i,j} = \mathbf{v}_t$ ).  $\mathbf{p}_t = [p_t^1, p_t^2, \dots, p_t^D] \in \mathbb{R}^D$  denotes the perturbation applied to timestamp  $t$  and remains identical across all overlapping samples ( $\delta_{n,l} = \delta_{i,j} = \mathbf{p}_t$ ), where  $p_t^d$  is the perturbation for the  $d$ -th variable  $v_t^d$  at timestamp  $t$  with  $|p_t^d| \leq \epsilon \cdot |v_t^d|$ .*

Under the commonly applied non-stride sliding-window sampling mechanism for constructing the time series forecasting dataset  $\mathcal{D}$ , this definition is equivalent to imposing two additional constraints on Definition 1. The first constraint

ensures temporal consistency that, for any adjacent samples  $\mathbf{x}_n, \mathbf{x}_{n+1} \in \mathcal{S}$ , we require  $\delta_{n,l+1} = \delta_{n+1,l} = \mathbf{p}_{n+l}$  to ensure that the same timestamp receives shared perturbations across overlapping samples. The second constraint ensures magnitude imperceptibility that, the perturbation  $\mathbf{p}_t$  for each timestamp  $t$  is variable-wisely bounded by a percentage  $\epsilon$  of the corresponding input value  $\mathbf{v}_t$  as  $|p_t^d| \leq \epsilon \cdot |v_t^d|$  for all  $v_t^d \in \mathbf{v}_t$ .

### 3.3 Adversarial Perturbation Generation

Let  $\tau$  denote the starting timestamp of the test dataset  $\mathcal{S} = \{(\mathbf{x}_n, \mathbf{y}_n)\}_{n=\tau}^N$ . Given a timestamp  $t$  covered in  $\mathcal{S}$ , i.e.,  $\tau \leq t \leq N + L - 1$ , let  $\mathcal{T}_t = \{(\mathbf{x}_i, \mathbf{y}_i) \in \mathcal{S} \mid \mathbf{v}_t \in \mathbf{x}_i\}$  denote the set of overlapping samples whose inputs contain the observed value  $\mathbf{v}_t$ , such as  $\mathcal{T}_\tau = \{(\mathbf{x}_\tau, \mathbf{y}_\tau)\}$  and  $\mathcal{T}_{\tau+1} = \{(\mathbf{x}_i, \mathbf{y}_i)\}_{i=\tau}^{\tau+1}$ . The adversarial objective under the TUAP constraints at timestamp  $t$  can be defined as:

$$\begin{aligned} \delta_n^* &= [\mathbf{p}_n^*, \mathbf{p}_{n+1}^*, \dots, \mathbf{p}_t^*, \dots, \mathbf{p}_{n+L-1}^*], \\ \mathbf{p}_t^* &= \underset{\mathbf{p}_t}{\operatorname{argmax}} \sum_{\mathbf{x}_i \in \mathcal{T}_t} \mathcal{L}(f_\theta(\mathbf{x}_i + \delta_i), \mathbf{y}_i), \quad \text{s.t. } \forall p_t^d \in \mathbf{p}_t, |p_t^d| \leq \epsilon \cdot |v_t^d|. \end{aligned} \quad (15)$$

Notably, optimizing  $\mathbf{p}_t$  for sample  $\mathbf{x}_n$  in Eq. (15) requires the adversarial perturbations  $\delta_i$  of other overlapping samples  $\mathbf{x}_i \in \mathcal{T}_t$ , making it challenging to ensure the TUAP property while simultaneously perturbing multiple samples with cascading effects.

To address this, it is intuitive and effective to calculate perturbations per timestamp rather than per sample, since a perturbation  $\mathbf{p}_t$  at a specific timestamp  $t$  is unique and simultaneously affects all samples whose time range covers  $t$ . Thus, we develop the Timestamp-wise Gradient Sign Method (TGSM), which provides a straightforward approach by optimizing each timestamp independently without considering perturbations at other timestamps.

Specifically, TGSM solves the optimization problem in Eq. (15) by performing a single-step gradient ascent on the loss function with respect to the perturbation  $\mathbf{p}_t$  at timestamp  $t$ . Let  $\check{\delta}_{i,t}$  denote a zero vector with the same shape as  $\mathbf{x}_i$  except that the value at timestamp  $t$  is replaced by  $\mathbf{p}_t$ . Then, the optimal perturbation  $\mathbf{p}_t$  can be calculated as:

$$\begin{aligned} \mathbf{p}_t &= \epsilon \cdot \operatorname{sign}(\mathbf{g}_t) \cdot \mathbf{v}_t, \\ \mathbf{g}_t &= \nabla_{\mathbf{v}_t} \sum_{\mathbf{x}_i \in \mathcal{T}_t} \mathcal{L}(f_\theta(\mathbf{x}_i + \check{\delta}_{i,t}), \mathbf{y}_i). \end{aligned} \quad (16)$$

By calculating  $\mathbf{p}_t$  for each timestamp  $t \in \{n, n+1, \dots, n+L-1\}$ , the adversarial example can be generated as  $\mathbf{x}'_n = \mathbf{x}_n + \mathbf{p}_{n:n+L-1}$ . Through sequentially calculating and caching the perturbation  $\mathbf{p}_t$  at historical timestamps, for subsequent input samples such as  $\mathbf{x}_{n+1}$ , TGSM only needs to calculate the perturbation  $\mathbf{p}_{n+L}$  for the new observation  $\mathbf{v}_{n+L}$ .

However, TGSM has several limitations. First, TGSM does not share the same computational advantage as traditional FGSM. Let  $\mathcal{O}(1)$  denote a single forward and backward propagation for calculating the gradient on the input sample  $\mathbf{x}_i$ , the time complexity of TGSM for generating all  $\mathbf{p}_{\tau:N+L-1}$  in the test set  $\mathcal{S}$  is  $\mathcal{O}(L \cdot |\mathcal{S}|)$ , leading to an average time complexity of  $\mathcal{O}(L)$  per sample, whereas FGSM has  $\mathcal{O}(1)$  complexity per sample. Second, this single-step approach ignores the non-convex curvature of the DNN's loss landscape. More importantly, it always uses the gradient direction at the original input  $\mathbf{x}$  and ignores the perturbations at historical timestamps, which may lead to suboptimal attack performance.

To address these issues, we propose the Timestamp-wise Gradient Accumulation Method (TGAM), which performs multi-step iterative optimization with gradient accumulation. Let  $\delta_i^k$  denote the perturbation for sample  $\mathbf{x}_i$  at iteration  $k$ , which is sliced from the timestamp-level perturbations as  $\delta_i^k = \mathbf{p}_{i:i+L-1}^k$ .  $\mathbf{v}_t'^k$  denotes the adversarial example of  $\mathbf{v}_t$  at iteration  $k$ , constructed as  $\mathbf{v}_t'^k = \mathbf{v}_t + \mathbf{p}_t^k$ . We sequentially calculate the gradient  $\mathbf{g}_t^k$  for all timestamps  $t$  at iteration  $k$  as:

$$\mathbf{g}_t^k = \sum_{\mathbf{x}_i \in \mathcal{T}_t} \nabla_{\mathbf{v}_t'^k} \mathcal{L}(f_\theta(\mathbf{x}_i'^k), \mathbf{y}_n), \quad (17)$$

where  $\mathbf{x}_i'^k = \mathbf{x}_i + \delta_i^k = \mathbf{x}_i + \mathbf{p}_{i:i+L-1}^k$ .

The proposed TGAM offers several benefits. First, by performing multi-step optimization, TGAM can better navigate the non-convex loss landscape of DNNs, leading to stronger adversarial perturbations. Second, TGAM is simple, modular, and can be easily integrated with various momentum-based optimization techniques to further improve attack performance and transferability. Third, the gradient accumulation mechanism allows TGAM to leverage the collective gradient information from all overlapping samples, which shares similar insights with input transformation-based

attacks, thereby enhancing attack effectiveness by finding a more optimal perturbation direction that considers the interactions between samples.

Moreover, TGAM is computationally efficient. Unlike existing input transformation-based attacks that require generating new transformed samples for each input, TGAM cleverly leverages the inherent structure of time series forecasting by using overlapping input samples as natural transformations for the current sample. This avoids the additional overhead incurred by introducing extra samples in input transformation approaches. Consequently, TGAM achieves an overall time complexity of  $\mathcal{O}(|\mathcal{S}|)$  for generating all perturbations  $\mathbf{p}_{\tau:N+L-1}^k$  in  $\mathcal{S}$ , demonstrating computational efficiency comparable to traditional methods such as PGD.

### 3.4 Implementation of Attacking Algorithm

As discussed above, TGAM provides a modular framework to improve attack performance for time series forecasting. To illustrate this, we present MI-TGAM, which incorporates the momentum-based update mechanism of MI-FGSM [18] into TGAM. MI-FGSM has been a standard baseline attack algorithm for follow-up works, making it a natural choice for demonstrating the effectiveness of our approach.

In contrast to traditional MI-FGSM, which computes the gradient for each sample independently, MI-TGAM sequentially computes the gradient for each timestamp by aggregating the gradients from all overlapping samples. For each iteration  $k$ , we first update the adversarial example  $\mathbf{x}_n'^k = \mathbf{x}_n + \mathbf{p}_{n:n+L-1}^k$  for each input sample  $\mathbf{x}_n \in \mathcal{S}$  by concatenating the current timestamp-level perturbations. Then, we calculate the sample-level gradient  $\mathbf{c}_n^k \in \mathbb{R}^{L \times D}$  for each sample  $\mathbf{x}_n'^k$  via backpropagation as:

$$\mathbf{c}_n^k = \nabla_{\mathbf{x}_n'^k} \mathcal{L}(f_\theta(\mathbf{x}_n'^k), \mathbf{y}_n), \quad (18)$$

collecting the gradient cache  $\mathcal{C}^k = \{\mathbf{c}_n^k\}_{n=\tau}^N$  for the attacking set  $\mathcal{S}$ .

Next, we perform timestamp-wise accumulation of the sample-level gradients to obtain the global gradient  $\mathbf{g}_t^k$  for each timestamp  $t$  as in Eq. (17). For brevity, we illustrate this gradient accumulation process with a commonly used practice that the samples are generated without strides. Specifically, let  $\mathbf{c}_{n,l}^k$  denote the  $l$ -th gradient vector in  $\mathbf{c}_n^k = [\mathbf{c}_{n,1}^k, \mathbf{c}_{n,2}^k, \dots, \mathbf{c}_{n,L}^k]$  corresponding to the  $l$ -th time step of the input sample  $\mathbf{x}_n'^k$ , which is associated with timestamp  $t = n + l - 1$ . Taking into account the boundary conditions of the test set, the global gradient for timestamp  $t$  is then computed by accumulating all sample-level gradients at that timestamp as:

$$\mathbf{g}_t^k = \begin{cases} \sum_{l=1}^{t-\tau+1} \mathbf{c}_{t-l+1,l}^k & \text{when } \tau + L - 1 > t \geq \tau, \\ \sum_{l=1}^L \mathbf{c}_{t-l+1,l}^k & \text{when } N \geq t \geq \tau + L - 1, \\ \sum_{j=t-L+1}^N \mathbf{c}_{j,t-j+1}^k & \text{when } N + L - 1 \geq t > N. \end{cases} \quad (19)$$

Through this process, we construct the temporally unified gradient  $\mathbf{g}_{\tau:N+L-1}^k$  for the entire attack set.

Finally, we update the timestamp-level perturbation  $\mathbf{p}_t^k$  by performing a momentum-based update with the accumulated gradient  $\mathbf{c}_n^k$  for each timestamp  $t$ , as follows:

$$\begin{aligned} \mathbf{p}_t^{k+1} &= \text{clip}(\mathbf{p}_t^k + \alpha \cdot \text{sign}(\boldsymbol{\omega}_t^k) \cdot \mathbf{v}_t, \epsilon \cdot \mathbf{v}_t), \\ \boldsymbol{\omega}_t^{k+1} &= \mu \cdot \boldsymbol{\omega}_t^k + \frac{\mathbf{g}_t^k}{\|\mathbf{g}_t^k\|_1}, \end{aligned} \quad (20)$$

where  $\boldsymbol{\omega}_t^k$  is the momentum term for timestamp  $t$  at iteration  $k$ . After  $K$  iterations, the optimized perturbation series  $\mathbf{p}_{\tau:N+L-1} \leftarrow \mathbf{p}_{\tau:N+L-1}^K$  is sliced back into sample-level perturbations  $\boldsymbol{\delta}_n = \mathbf{p}_{n:n+L-1}$  for each sample  $\mathbf{x}_n \in \mathcal{S}$ , forming the final TUAPs.

Through this implementation, MI-TGAM effectively exploits gradient information from multi-step optimization while maintaining the temporally unified constraint, resolving the temporally inconsistent perturbations problem while enhancing attack effectiveness for time series forecasting.

## 4 Experiment

### 4.1 Experimental Setup

**Datasets.** To evaluate the attack performance in different application scenarios under the definition of temporally unified adversarial perturbations, we conduct experiments on three commonly used real-world time series datasets [12,

13, 27, 28]: ETT<sup>3</sup>(electricity transformers dataset ETTh1), Electricity<sup>4</sup> (electricity consumption dataset), and Traffic<sup>5</sup> (road occupancy dataset). For each dataset, we use 70% of the data for training, 10% for validation, and 20% for testing, following the standard split protocol in time series forecasting literature. The test set is used as the attack set for evaluating attack performance.

**Models.** To validate the effectiveness and generalization of the attacks across different neural architectures, we select four state-of-the-art time series forecasting models with representative structures: the MLP-based FreTS [27], the RNN-based SegRNN [28], the CNN-based TimesNet [12], and the Transformer-based iTransformer [13].

**Baselines.** We compare the proposed method (MI-TGAM) with several representative methods: FGSM [5], BIM [16], PGD [17], MI-FGSM [18], ATSG [9], ADJM [11], TCA [10], and BO [24]. Among these baselines, FGSM, BIM, PGD, and MI-FGSM are general adversarial attack methods widely used in computer vision, while ATSG, ADJM, TCA, and BO are specifically designed for time series forecasting tasks. Notably, all these methods optimize perturbations for individual samples independently, which inherently leads to temporally inconsistent perturbations where the same timestamp receives contradictory values across different samples. For fair comparison, we adapt these methods to satisfy the TUAP constraint by randomly selecting one perturbation from the overlapping samples for each shared timestamp.

**Attack Settings.** Following prior works [9, 10], we use the  $L_\infty$  norm to constrain the maximum perturbation magnitude. For each variable in the input time series, we set the perturbation budget  $\epsilon = 0.1$ , which limits the perturbation to 10% of the original magnitude for each variable:  $|p_t^d| \leq \epsilon \cdot |v_t^d|$ . For iterative attack methods (including ours), we set the number of iterations  $K = 10$  and the step size  $\alpha = \epsilon/K = 0.01$ . For momentum-based methods, we set the decay factor  $\mu = 1.0$  following MI-FGSM [18]. For other hyperparameters specific to each baseline method, we follow the settings in their original papers. For the forecasting tasks, we set both the input length  $L$  and the prediction horizon  $H$  to 96, which is a standard setting in time series forecasting literature.

We adopt a cross-model transfer attack evaluation protocol, where each of the four models is used in turn as a surrogate model to generate adversarial examples that are then used to attack the other three target models. When the surrogate model and target model are the same, the setting corresponds to a white-box attack; when they differ, the setting corresponds to a black-box transfer attack. The attack performance is evaluated using two metrics: Mean Squared Error (MSE) and Mean Absolute Error (MAE). To more clearly compare the attack effectiveness, we also report the degradation percentage, calculated as:

$$\text{Degradation}(\%) = \frac{\text{Error}_{\text{Attack}} - \text{Error}_{\text{Clean}}}{\text{Error}_{\text{Clean}}} \times 100\%, \quad (21)$$

where  $\text{Error}_{\text{Attack}}$  is the error on adversarial examples and  $\text{Error}_{\text{Clean}}$  is the error on clean data. A higher degradation percentage indicates a stronger attack.

## 4.2 White-box Attack Results

The white-box attack results are summarized in Table 1, where the original forecasting performance without any attacks is reported as “Clean”, and the mean performance across the four models for each attack method is presented in the “Average” column. The results show that MI-TGAM consistently and significantly outperforms all baseline methods across all three benchmark datasets and four distinct model architectures, demonstrating the superiority of our method in identifying adversarial vulnerabilities in time series forecasting models.

Compared to traditional iterative attack methods such as BIM, PGD, and MI-FGSM, our MI-TGAM exhibits superior performance by leveraging the inherent characteristics of time series forecasting, which utilizes overlapping samples to enrich gradient information through timestamp-wise accumulation. Compared to specialized time series attack methods, including ATSG, ADJM, TCA, and BO, MI-TGAM also significantly outperforms these baselines by maintaining temporal consistency while maximizing prediction errors. Notably, MI-TGAM is the only method that consistently amplifies prediction errors across all target models and datasets. For instance, when attacking SegRNN on the Traffic dataset, PGD, ATSG, ADJM, TCA, and BO all fail to degrade performance (with some even improving the MSE), while MI-TGAM significantly degrades SegRNN’s performance, demonstrating its exceptional attack effectiveness.

<sup>3</sup><https://github.com/zhouhaoyi/ETDataset>

<sup>4</sup><https://archive.ics.uci.edu/dataset/321/electricityloaddiagrams20112014>

<sup>5</sup><https://pems.dot.ca.gov/>

Table 1: White-box attack results of for MI-TGAM and baseline methods across four models and three datasets. Best results are highlighted in **bold**.

Dataset	Method	MSE (with Degradation Percentage)					MAE (with Degradation Percentage)				
		FreTS	SegRNN	TimesNet	iTransformer	Average	FreTS	SegRNN	TimesNet	iTransformer	Average
ETT	Clean	0.411 (-0.0%)	0.377 (-0.0%)	0.446 (-0.0%)	0.398 (-0.0%)	0.408 (-0.0%)	0.420 (-0.0%)	0.400 (-0.0%)	0.452 (-0.0%)	0.412 (-0.0%)	0.421 (-0.0%)
	FGSM	0.440 (7.1%)	0.401 (7.6%)	0.474 (7.6%)	0.417 (7.6%)	0.433 (7.6%)	0.443 (7.5%)	0.419 (7.4%)	0.463 (7.4%)	0.424 (7.9%)	0.437 (7.9%)
	BIM	0.440 (7.1%)	0.401 (7.6%)	0.478 (7.0%)	0.416 (7.5%)	0.434 (7.3%)	0.443 (7.5%)	0.419 (7.4%)	0.464 (7.2%)	0.423 (7.7%)	0.437 (7.9%)
	PGD	0.432 (5.1%)	0.394 (7.4%)	0.469 (7.0%)	0.412 (7.4%)	0.427 (7.6%)	0.436 (7.3%)	0.414 (7.3%)	0.460 (7.8%)	0.421 (7.1%)	0.433 (7.8%)
	MI-FGSM	0.440 (7.1%)	0.402 (7.6%)	0.478 (7.2%)	0.417 (7.7%)	0.434 (7.4%)	0.443 (7.5%)	0.420 (7.0%)	0.464 (7.2%)	0.424 (7.9%)	0.438 (7.4%)
	ATSG	0.438 (6.6%)	0.400 (7.6%)	0.472 (5.8%)	0.415 (7.1%)	0.431 (7.0%)	0.433 (7.6%)	0.421 (5.3%)	0.461 (7.2%)	0.425 (7.1%)	0.438 (4.1%)
	ADJM	0.411 (7.0%)	0.382 (7.4%)	0.451 (7.0%)	0.401 (7.0%)	0.411 (7.0%)	0.424 (7.1%)	0.407 (7.1%)	0.454 (7.0%)	0.415 (7.0%)	0.425 (1.0%)
ECL	TCA	0.436 (7.2%)	0.397 (7.5%)	0.474 (7.6%)	0.414 (7.8%)	0.440 (7.5%)	0.442 (7.2%)	0.419 (7.7%)	0.464 (7.2%)	0.424 (7.9%)	0.437 (3.8%)
	BO	0.415 (7.0%)	0.377 (7.0%)	0.450 (7.0%)	0.405 (7.1%)	0.412 (7.0%)	0.427 (7.1%)	0.401 (7.0%)	0.457 (7.1%)	0.420 (7.1%)	0.426 (1.2%)
	MI-TGAM	<b>0.454 (7.0%)</b>	<b>0.416 (7.0%)</b>	<b>0.508 (7.3%)</b>	<b>0.431 (7.1%)</b>	<b>0.452 (7.0%)</b>	<b>0.454 (7.8%)</b>	<b>0.434 (7.4%)</b>	<b>0.475 (7.1%)</b>	<b>0.434 (7.3%)</b>	<b>0.449 (7.6%)</b>
	Clean	0.195 (-0.0%)	0.206 (-0.0%)	0.259 (-0.0%)	0.154 (-0.0%)	0.204 (-0.0%)	0.283 (-0.0%)	0.291 (-0.0%)	0.341 (-0.0%)	0.245 (-0.0%)	0.290 (-0.0%)
	FGSM	0.212 (7.8%)	0.223 (7.8%)	0.276 (7.6%)	0.168 (7.8%)	0.220 (7.8%)	0.305 (7.6%)	0.311 (7.0%)	0.357 (7.4%)	0.261 (7.3%)	0.308 (7.3%)
	BIM	0.212 (7.8%)	0.223 (7.8%)	0.277 (7.9%)	0.163 (7.8%)	0.219 (7.5%)	0.305 (7.6%)	0.311 (7.0%)	0.357 (7.4%)	0.255 (7.3%)	0.307 (7.5%)
	PGD	0.207 (7.4%)	0.219 (7.1%)	0.270 (7.4%)	0.162 (7.2%)	0.214 (5.4%)	0.299 (5.6%)	0.306 (5.2%)	0.351 (12.7%)	0.254 (13.6%)	0.302 (4.2%)
	MI-FGSM	0.212 (7.8%)	0.224 (7.6%)	0.279 (7.6%)	0.168 (7.7%)	0.221 (7.4%)	0.305 (7.6%)	0.312 (7.3%)	0.359 (15.1%)	0.260 (16.0%)	0.309 (6.5%)
Traffic	ATSG	0.211 (7.3%)	0.222 (7.8%)	0.277 (7.1%)	0.167 (8.0%)	0.219 (7.7%)	0.306 (8.1%)	0.310 (7.3%)	0.361 (15.9%)	0.263 (17.0%)	0.311 (7.0%)
	ADJM	0.198 (7.1%)	0.211 (7.2%)	0.257 (7.0%)	0.157 (12.1%)	0.206 (11.1%)	0.290 (2.6%)	0.301 (3.4%)	0.339 (7.0%)	0.251 (12.2%)	0.295 (1.7%)
	TCA	0.209 (7.4%)	0.220 (7.6%)	0.280 (7.1%)	0.162 (5.0%)	0.218 (7.0%)	0.304 (7.3%)	0.310 (6.5%)	0.362 (6.0%)	0.255 (13.9%)	0.308 (6.0%)
	BO	0.196 (7.0%)	0.207 (7.0%)	0.256 (7.1%)	0.155 (7.0%)	0.204 (7.0%)	0.285 (7.0%)	0.292 (7.0%)	0.338 (9.0%)	0.247 (10.8%)	0.291 (1.2%)
	MI-TGAM	<b>0.225 (7.5%)</b>	<b>0.237 (14.8%)</b>	<b>0.322 (24.2%)</b>	<b>0.240 (55.6%)</b>	<b>0.256 (25.7%)</b>	<b>0.319 (12.7%)</b>	<b>0.328 (12.7%)</b>	<b>0.395 (15.7%)</b>	<b>0.313 (27.5%)</b>	<b>0.339 (16.7%)</b>
	Clean	0.564 (-0.0%)	0.694 (-0.0%)	0.611 (-0.0%)	0.412 (-0.0%)	0.570 (-0.0%)	0.378 (-0.0%)	0.355 (-0.0%)	0.333 (-0.0%)	0.283 (-0.0%)	0.336 (-0.0%)
	FGSM	0.592 (4.8%)	0.696 (0.3%)	0.634 (3.8%)	0.429 (4.1%)	0.588 (3.1%)	0.396 (4.9%)	0.354 (0.5%)	0.345 (3.8%)	0.295 (4.2%)	0.348 (3.3%)
	BIM	0.592 (7.4%)	0.696 (0.3%)	0.634 (3.8%)	0.429 (4.1%)	0.588 (3.1%)	0.396 (4.9%)	0.354 (0.5%)	0.345 (3.8%)	0.295 (4.2%)	0.348 (3.3%)
ECL	PGD	0.585 (3.6%)	0.688 (0.8%)	0.628 (2.8%)	0.424 (3.1%)	0.581 (1.9%)	0.391 (3.5%)	0.349 (1.0%)	0.342 (2.8%)	0.291 (3.0%)	0.343 (2.1%)
	MI-FGSM	0.592 (4.8%)	0.696 (0.3%)	0.634 (3.8%)	0.429 (3.1%)	0.588 (3.1%)	0.396 (4.9%)	0.354 (0.5%)	0.345 (3.8%)	0.295 (4.2%)	0.348 (3.3%)
	ATSG	0.587 (4.1%)	0.689 (0.7%)	0.630 (3.2%)	0.426 (3.5%)	0.583 (2.3%)	0.397 (5.3%)	0.357 (1.1%)	0.349 (4.8%)	0.299 (5.8%)	0.350 (4.2%)
	ADJM	0.569 (0.8%)	0.677 (12.4%)	0.618 (1.2%)	0.413 (0.4%)	0.569 (0.1%)	0.382 (1.2%)	0.344 (2.5%)	0.341 (2.4%)	0.286 (1.1%)	0.338 (0.5%)
	TCA	0.587 (4.1%)	0.689 (0.7%)	0.630 (3.2%)	0.426 (3.5%)	0.583 (2.3%)	0.397 (5.3%)	0.357 (1.1%)	0.349 (4.8%)	0.299 (5.8%)	0.350 (4.2%)
	BO	0.565 (0.2%)	0.668 (13.8%)	0.613 (0.4%)	0.412 (0.2%)	0.565 (1.0%)	0.379 (0.3%)	0.337 (4.5%)	0.335 (10.8%)	0.284 (10.6%)	0.334 (0.8%)
	MI-TGAM	<b>0.613 (8.5%)</b>	<b>0.722 (4.0%)</b>	<b>0.705 (15.5%)</b>	<b>0.459 (11.4%)</b>	<b>0.625 (9.5%)</b>	<b>0.410 (8.5%)</b>	<b>0.371 (5.2%)</b>	<b>0.384 (15.4%)</b>	<b>0.312 (10.4%)</b>	<b>0.369 (9.8%)</b>

Table 2: Averaged Transfer attack results of MI-TGAM and baseline methods with four surrogate models.

Dataset	Method	Degradation Percentage on MSE					Degradation Percentage on MAE				
		FreTS	SegRNN	TimesNet	iTransformer	Average	FreTS	SegRNN	TimesNet	iTransformer	Average
ETT	FGSM	<b>5.75%</b>	<b>5.88%</b>	2.71%	2.77%	4.28%	4.48%	4.40%	1.92%	1.57%	3.09%
	BIM	<b>5.75%</b>	<b>5.83%</b>	2.58%	2.70%	4.21%	4.47%	4.36%	1.77%	1.46%	3.02%
	PGD	4.17%	4.30%	1.91%	2.02%	3.10%	3.30%	3.31%	1.35%	1.08%	2.26%
	MI-FGSM	<b>5.75%</b>	<b>5.95%</b>	2.72%	2.83%	4.31%	4.47%	4.47%	1.92%	1.56%	3.11%
	ATSG	5.47%	5.60%	2.57%	2.50%	4.04%	4.66%	4.64%	1.99%	1.65%	3.23%
	ADJM	1.80%	1.04%	0.688	0.31%	0.96%	2.20%	1.74%	0.81%	0.23%	1.24%
	TCA	5.06%	4.81%	2.13%	2.35%	3.59%	4.31%	4.07%	1.63%	1.58%	2.90%
ECL	BO	0.88%	1.19%	1.00%	0.72%	0.95%	1.44%	1.72%	1.47%	0.89%	1.38%
	MI-TGAM	<b>8.14%</b>	<b>9.03%</b>	<b>4.03%</b>	<b>4.73%</b>	<b>6.48%</b>	<b>6.31%</b>	<b>7.17%</b>	<b>3.01%</b>	<b>2.97%</b>	<b>4.86%</b>
	FGSM	5.95%	6.25%	3.76%	1.62%	4.39%	5.11%	5.14%	3.26%	1.60%	3.78%
	BIM	6.01%	6.16%	2.09%	0.63%	3.72%	5.15%	5.02%	1.86%	0.50%	3.13%
	PGD	4.23%	4.43%	1.60%	0.57%	2.71%	3.59%	3.61%	1.41%	0.52%	2.28%
	MI-FGSM	5.99%	6.47%	2.78%	1.33%	4.14%	5.15%	5.37%	2.44%	1.23%	3.55%
	ATSG	5.64%	5.86%	3.21%	1.57%	4.07%	5.46%	5.30%	3.51%	1.94%	4.05%
Traffic	ADJM	1.82%	1.72%	1.23%	0.27%	1.26%	2.74%	2.72%	1.42%	0.50%	1.84%
	TCA	4.73%	4.88%	1.80%	0.49%	2.98%	4.70%	4.34%	1.93%	0.59%	2.89%
	BO	-0.13%	-0.06%	0.53%	-0.12%	0.05%	0.01%	0.08%	0.63%	0.01%	0.18%
	MI-TGAM	<b>10.92%</b>	<b>11.36%</b>	<b>5.56%</b>	<b>4.11%</b>	<b>7.99%</b>	<b>9.10%</b>	<b>9.49%</b>	<b>5.22%</b>	<b>3.64%</b>	<b>6.86%</b>
	FGSM	0.64%	2.37%	-0.69%	-0.02%	0.58%	1.48%	3.00%	-0.46%	0.16%	1.04%
	BIM	0.64%	2.37%	-0.69%	-0.02%	0.58%	1.48%	3.00%	-0.46%	0.16%	1.04%
	PGD	0.06%	1.76%	-0.96%	-0.39%	0.12%	0.59%	2.18%	-0.86%	-0.31%	0.40%
Traffic	MI-FGSM	0.64%	2.37%	-0.69%	-0.02%	0.58%	1.48%	3.00%	-0.46%	0.16%	1.04%
	ATSG	0.60%	2.14%	-0.81%	-0.11%	0.45%	1.96%	3.57%	-0.44%	0.55%	1.41%
	ADJM	-0.63%	0.82%	-1.20%	-1.06%	-0.52%	-0.07%	2.02%	-0.74%	-0.83%	0.09%
	TCA	0.60%	2.14%	-0.81%	-0.11%	0.45%	1.96%	3.57%	-0.44%	0.55%	1.41%
	BO	-1.34%	0.24%	-1.46%	-1.23%	-0.95%	-1.19%	0.56%	-1.28%	-1.12%	-0.76%
	MI-TGAM	<b>2.21%</b>	<b>4.21%</b>	<b>0.39%</b>	<b>1.53%</b>	<b>2.09%</b>	<b>3.99%</b>	<b>5.37%</b>	<b>1.42%</b>	<b>2.03%</b>	<b>3.20%</b>

### 4.3 Transfer Attack Results

To evaluate the adversarial transferability of the attack methods, we conduct a comprehensive evaluation of transfer attack performance across different surrogate-target model pairs. The overall results are summarized in Table 2, where each entry under a surrogate model column represents the average MSE/MAE degradation percentage across the other three target models, and the entry under the “Average” column denotes the mean degradation percentage across all black-box transfer attack scenarios for each method. The results clearly show that MI-TGAM significantly outperforms all baseline methods in terms of transfer attack performance, achieving nearly double the degradation percentage of the second-best method, demonstrating the superior transferability of the adversarial examples generated by MI-TGAM.

We also present detailed transfer attack results for each surrogate model in Table 3, Table 4, Table 5, and Table 6, where the average MSE/MAE degradation percentage across all three target models is reported for each dataset. The

Table 3: Transfer attack results of MI-TGAM and baseline methods using FrTS as the surrogate model.

Dataset	Method	Target Model (Using FrTS as Surrogate Model)							
		MSE (with Degradation Percentage)				MAE (with Degradation Percentage)			
		SegRNN	TimesNet	iTransformer	Average	SegRNN	TimesNet	iTransformer	Average
ETT	Clean	0.377 (-0.0%)	0.446 (-0.0%)	0.398 (-0.0%)	0.407 (-0.0%)	0.400 (-0.0%)	0.452 (-0.0%)	0.412 (-0.0%)	0.421 (-0.0%)
	FGSM	0.401 (↑6.4%)	0.464 (↑4.0%)	0.426 (↑7.0%)	0.430 (↑5.7%)	0.419 (↑4.8%)	0.464 (↑2.6%)	0.433 (↑5.1%)	0.439 (↑4.1%)
	BIM	0.401 (↑6.4%)	0.464 (↑4.0%)	0.426 (↑7.0%)	0.430 (↑5.7%)	0.419 (↑4.8%)	0.464 (↑2.6%)	0.433 (↑5.1%)	0.439 (↑4.1%)
	PGD	0.394 (↑4.6%)	0.459 (↑2.9%)	0.419 (↑5.1%)	0.424 (↑4.2%)	0.414 (↑3.4%)	0.461 (↑1.8%)	0.427 (↑3.7%)	0.434 (↑3.0%)
	MI-FGSM	0.401 (↑6.4%)	0.464 (↑4.0%)	0.426 (↑7.0%)	0.430 (↑5.7%)	0.419 (↑4.8%)	0.464 (↑2.6%)	0.433 (↑5.1%)	0.439 (↑4.1%)
	ATSG	0.400 (↑6.1%)	0.463 (↑3.7%)	0.425 (↑6.7%)	0.429 (↑5.4%)	0.420 (↑5.1%)	0.464 (↑2.6%)	0.434 (↑5.4%)	0.440 (↑4.3%)
	ADIM	0.383 (↑1.9%)	0.454 (↑1.7%)	0.406 (↑1.8%)	0.414 (↑1.8%)	0.408 (↑2.1%)	0.460 (↑1.7%)	0.420 (↑1.8%)	0.429 (↑1.9%)
	TCA	0.398 (↑5.8%)	0.461 (↑3.4%)	0.423 (↑6.3%)	0.428 (↑5.0%)	0.419 (↑4.7%)	0.463 (↑2.3%)	0.433 (↑5.0%)	0.438 (↑4.0%)
	BO	0.377 (↑0.1%)	0.450 (↑0.8%)	0.405 (↑1.6%)	0.411 (↑0.9%)	0.401 (↑0.3%)	0.457 (↑1.1%)	0.420 (↑1.8%)	0.426 (↑1.1%)
ECL	MI-TGAM	<b>0.411 (↑9.2%)</b>	<b>0.471 (↑5.6%)</b>	<b>0.438 (↑9.9%)</b>	<b>0.440 (↑8.1%)</b>	<b>0.428 (↑7.0%)</b>	<b>0.469 (↑3.8%)</b>	<b>0.442 (↑7.2%)</b>	<b>0.446 (↑5.9%)</b>
Traffic	Clean	0.206 (-0.0%)	0.259 (-0.0%)	0.154 (-0.0%)	0.206 (-0.0%)	0.291 (-0.0%)	0.341 (-0.0%)	0.245 (-0.0%)	0.293 (-0.0%)
	FGSM	0.221 (↑7.4%)	0.266 (↑2.6%)	0.169 (↑9.7%)	0.219 (↑6.0%)	0.310 (↑6.4%)	0.347 (↑1.8%)	0.265 (↑8.2%)	0.307 (↑5.1%)
	BIM	0.221 (↑7.4%)	0.266 (↑2.7%)	0.169 (↑9.7%)	0.219 (↑6.0%)	0.310 (↑6.5%)	0.348 (↑1.9%)	0.265 (↑8.1%)	0.308 (↑5.2%)
	PGD	0.217 (↑5.4%)	0.263 (↑1.6%)	0.165 (↑7.0%)	0.215 (↑4.2%)	0.304 (↑4.7%)	0.345 (↑1.0%)	0.260 (↑5.8%)	0.303 (↑3.6%)
	MI-FGSM	0.221 (↑7.4%)	0.266 (↑2.6%)	0.169 (↑9.7%)	0.219 (↑6.0%)	0.310 (↑6.5%)	0.348 (↑1.8%)	0.265 (↑8.2%)	0.308 (↑5.1%)
	ATSG	0.221 (↑7.0%)	0.265 (↑2.4%)	0.168 (↑9.3%)	0.218 (↑5.6%)	0.311 (↑6.9%)	0.348 (↑2.0%)	0.267 (↑8.6%)	0.309 (↑5.5%)
	ADIM	0.210 (↑2.1%)	0.260 (↑0.6%)	0.160 (↑3.5%)	0.210 (↑1.8%)	0.300 (↑3.1%)	0.345 (↑1.0%)	0.257 (↑4.7%)	0.301 (↑2.7%)
	TCA	0.219 (↑6.3%)	0.263 (↑1.5%)	0.167 (↑8.1%)	0.216 (↑4.7%)	0.309 (↑6.2%)	0.346 (↑1.3%)	0.264 (↑7.6%)	0.306 (↑4.7%)
	BO	0.207 (↑0.3%)	0.256 (↑1.0%)	0.155 (↑0.7%)	0.206 (↑0.1%)	0.292 (↑0.5%)	0.338 (↑0.9%)	0.247 (↑0.8%)	0.293 (↑0.0%)
Traffic	MI-TGAM	<b>0.233 (↑12.9%)</b>	<b>0.273 (↑5.4%)</b>	<b>0.181 (↑17.5%)</b>	<b>0.229 (↑10.9%)</b>	<b>0.322 (↑10.9%)</b>	<b>0.355 (↑4.0%)</b>	<b>0.280 (↑14.0%)</b>	<b>0.319 (↑9.1%)</b>

Table 4: Transfer attack results of MI-TGAM and baseline methods using SegRNN as the surrogate model.

Dataset	Method	Target Model (Using SegRNN as Surrogate Model)							
		MSE (with Degradation Percentage)				MAE (with Degradation Percentage)			
		FrTS	TimesNet	iTransformer	Average	FrTS	TimesNet	iTransformer	Average
ETT	Clean	0.411 (-0.0%)	0.446 (-0.0%)	0.398 (-0.0%)	0.419 (-0.0%)	0.420 (-0.0%)	0.452 (-0.0%)	0.412 (-0.0%)	0.428 (-0.0%)
	FGSM	0.433 (↑5.5%)	0.468 (↑4.9%)	0.426 (↑6.9%)	0.442 (↑5.7%)	0.436 (↑3.8%)	0.466 (↑3.0%)	0.433 (↑5.1%)	0.445 (↑4.0%)
	BIM	0.433 (↑5.4%)	0.468 (↑4.8%)	0.426 (↑6.8%)	0.442 (↑5.7%)	0.436 (↑3.8%)	0.466 (↑3.0%)	0.433 (↑5.1%)	0.445 (↑3.9%)
	PGD	0.427 (↑3.9%)	0.462 (↑3.6%)	0.419 (↑5.0%)	0.436 (↑4.1%)	0.431 (↑2.7%)	0.462 (↑2.2%)	0.428 (↑3.7%)	0.440 (↑2.9%)
	MI-FGSM	0.434 (↑5.6%)	0.468 (↑4.9%)	0.426 (↑7.0%)	0.443 (↑5.8%)	0.436 (↑3.9%)	0.466 (↑3.1%)	0.434 (↑5.2%)	0.445 (↑4.0%)
	ATSG	0.433 (↑5.4%)	0.466 (↑4.4%)	0.425 (↑6.7%)	0.441 (↑5.4%)	0.437 (↑4.1%)	0.466 (↑3.0%)	0.435 (↑5.5%)	0.446 (↑4.2%)
	ADIM	0.410 (↓0.2%)	0.453 (↑1.5%)	0.404 (↑1.4%)	0.422 (↑0.9%)	0.423 (↑0.8%)	0.459 (↑1.6%)	0.418 (↑1.5%)	0.434 (↑1.3%)
	TCA	0.430 (↑4.6%)	0.463 (↑3.7%)	0.422 (↑5.8%)	0.438 (↑4.6%)	0.435 (↑3.6%)	0.464 (↑2.5%)	0.432 (↑4.8%)	0.444 (↑3.6%)
	BO	0.414 (↑0.7%)	0.450 (↑0.8%)	0.405 (↑1.6%)	0.423 (↑1.0%)	0.424 (↑0.9%)	0.457 (↑1.1%)	0.420 (↑1.8%)	0.434 (↑1.3%)
ECL	MI-TGAM	<b>0.447 (↑8.7%)</b>	<b>0.480 (↑7.5%)</b>	<b>0.441 (↑10.6%)</b>	<b>0.456 (↑8.9%)</b>	<b>0.448 (↑6.6%)</b>	<b>0.476 (↑5.2%)</b>	<b>0.447 (↑8.4%)</b>	<b>0.457 (↑6.7%)</b>
Traffic	Clean	0.195 (-0.0%)	0.259 (-0.0%)	0.154 (-0.0%)	0.203 (-0.0%)	0.283 (-0.0%)	0.341 (↓0.0%)	0.245 (-0.0%)	0.290 (↓0.0%)
	FGSM	0.210 (↑7.7%)	0.268 (↑3.3%)	0.169 (↑9.4%)	0.215 (↑6.2%)	0.301 (↑6.5%)	0.349 (↑2.2%)	0.264 (↑7.7%)	0.305 (↑5.1%)
	BIM	0.209 (↑7.5%)	0.268 (↑3.4%)	0.168 (↑9.1%)	0.215 (↑6.2%)	0.301 (↑6.3%)	0.349 (↑2.3%)	0.264 (↑7.4%)	0.305 (↑5.0%)
	PGD	0.206 (↑5.6%)	0.265 (↑2.2%)	0.165 (↑6.7%)	0.212 (↑4.4%)	0.296 (↑4.7%)	0.346 (↑1.4%)	0.259 (↑5.5%)	0.300 (↑3.6%)
	MI-FGSM	0.210 (↑7.8%)	0.268 (↑3.6%)	0.169 (↑9.6%)	0.216 (↑6.5%)	0.302 (↑6.7%)	0.349 (↑2.4%)	0.265 (↑8.0%)	0.306 (↑5.4%)
	ATSG	0.209 (↑7.3%)	0.267 (↑3.0%)	0.168 (↑8.9%)	0.215 (↑5.9%)	0.302 (↑6.8%)	0.349 (↑2.2%)	0.265 (↑7.9%)	0.305 (↑5.3%)
	ADIM	0.198 (↑1.7%)	0.261 (↑0.6%)	0.160 (↑3.6%)	0.206 (↑1.7%)	0.291 (↑2.7%)	0.345 (↑1.1%)	0.258 (↑5.0%)	0.298 (↑2.7%)
	TCA	0.207 (↑6.3%)	0.265 (↑2.3%)	0.166 (↑7.5%)	0.213 (↑4.9%)	0.299 (↑5.7%)	0.347 (↑1.6%)	0.261 (↑6.5%)	0.303 (↑4.3%)
	BO	0.196 (↑0.6%)	0.256 (↑1.0%)	0.155 (↑0.7%)	0.203 (↓0.1%)	0.285 (↑0.7%)	0.338 (↓0.9%)	0.247 (↑0.8%)	0.290 (↑0.1%)
Traffic	MI-TGAM	<b>0.221 (↑13.2%)</b>	<b>0.277 (↑6.9%)</b>	<b>0.180 (↑16.6%)</b>	<b>0.226 (↑11.4%)</b>	<b>0.315 (↑11.1%)</b>	<b>0.358 (↑4.9%)</b>	<b>0.280 (↑13.9%)</b>	<b>0.317 (↑9.5%)</b>

results show that MI-TGAM consistently achieves the highest transfer attack performance on almost all surrogate-target model pairs across all three datasets. The only exception is a small margin in MAE when attacking TimesNet using iTransformer as the surrogate model on the ETTh1 dataset. Overall, these results demonstrate the superior robustness and generalization capability of MI-TGAM for attacking various time series forecasting models in black-box settings.

#### 4.4 Sensitivity Analysis

To validate the robustness and stability of MI-TGAM under varying attack parameters and forecasting task configurations, we conduct a comprehensive sensitivity analysis on three key hyperparameters: the perturbation budget  $\epsilon$ , the number

Table 5: Transfer attack results of MI-TGAM and baseline methods using TimesNet as the surrogate model.

Dataset	Method	Target Model (Using TimesNet as Surrogate Model)							
		MSE (with Degradation Percentage)				MAE (with Degradation Percentage)			
		FrTS	SegRNN	iTransformer	Average	FrTS	SegRNN	iTransformer	Average
ETT	Clean	0.411 (-0.0%)	0.377 (-0.0%)	0.398 (-0.0%)	0.395 (-0.0%)	0.420 (-0.0%)	0.400 (-0.0%)	0.412 (-0.0%)	0.411 (-0.0%)
	FGSM	0.421 (↑2.5%)	0.385 (↑2.3%)	0.410 (↑2.9%)	0.405 (↑2.5%)	0.425 (↑1.2%)	0.406 (↑1.4%)	0.420 (↑1.8%)	0.417 (↑1.5%)
	BIM	0.420 (↑2.3%)	0.385 (↑2.2%)	0.409 (↑2.7%)	0.405 (↑2.4%)	0.424 (↑1.0%)	0.405 (↑1.3%)	0.419 (↑1.6%)	0.416 (↑1.3%)
	PGD	0.418 (↑1.6%)	0.382 (↑1.6%)	0.407 (↑2.0%)	0.402 (↑1.7%)	0.423 (↑0.6%)	0.403 (↑0.9%)	0.417 (↑1.1%)	0.414 (↑0.9%)
	MI-FGSM	0.421 (↑2.4%)	0.385 (↑2.3%)	0.410 (↑2.9%)	0.405 (↑2.6%)	0.425 (↑1.1%)	0.406 (↑1.5%)	0.420 (↑1.8%)	0.417 (↑1.5%)
	ATSG	0.420 (↑2.3%)	0.385 (↑2.2%)	0.409 (↑2.7%)	0.405 (↑2.4%)	0.425 (↑1.2%)	0.404 (↑1.6%)	0.420 (↑1.8%)	0.417 (↑1.5%)
	ADJM	0.412 (↑0.2%)	0.379 (↑0.5%)	0.402 (↑0.8%)	0.397 (↑0.5%)	0.420 (↑0.0%)	0.401 (↑0.4%)	0.415 (↑0.6%)	0.412 (↑0.4%)
	TCA	0.418 (↑1.8%)	0.384 (↑1.9%)	0.407 (↑2.2%)	0.403 (↑2.0%)	0.424 (↑0.9%)	0.405 (↑1.2%)	0.418 (↑1.4%)	0.415 (↑1.2%)
	BO	0.414 (↑0.7%)	0.377 (↑0.1%)	0.405 (↑1.6%)	0.399 (↑0.8%)	0.424 (↑0.9%)	0.401 (↑0.3%)	0.420 (↑1.8%)	0.415 (↑1.0%)
ECL	MI-TGAM	<b>0.426 (↑3.7%)</b>	<b>0.390 (↑3.6%)</b>	<b>0.416 (↑4.3%)</b>	<b>0.411 (↑3.9%)</b>	<b>0.429 (↑2.1%)</b>	<b>0.410 (↑2.6%)</b>	<b>0.424 (↑2.9%)</b>	<b>0.421 (↑2.5%)</b>
Traffic	Clean	0.195 (-0.0%)	0.206 (-0.0%)	0.154 (-0.0%)	0.185 (-0.0%)	0.283 (-0.0%)	0.291 (-0.0%)	0.245 (-0.0%)	0.273 (-0.0%)
	FGSM	0.202 (↑3.9%)	0.212 (↑2.6%)	0.162 (↑5.1%)	0.192 (↑3.8%)	0.292 (↑3.3%)	0.298 (↑2.4%)	0.256 (↑4.3%)	0.282 (↑3.3%)
	BIM	0.199 (↑2.1%)	0.209 (↑1.5%)	0.158 (↑2.8%)	0.189 (↑2.1%)	0.288 (↑1.9%)	0.295 (↑1.4%)	0.251 (↑2.4%)	0.278 (↑1.9%)
	PGD	0.198 (↑1.7%)	0.208 (↑1.1%)	0.158 (↑2.2%)	0.188 (↑1.6%)	0.287 (↑1.5%)	0.294 (↑1.0%)	0.250 (↑1.8%)	0.277 (↑1.4%)
	MI-FGSM	0.200 (↑2.9%)	0.210 (↑2.0%)	0.160 (↑3.8%)	0.190 (↑2.8%)	0.290 (↑2.4%)	0.296 (↑1.8%)	0.253 (↑3.2%)	0.280 (↑2.4%)
	ATSG	0.201 (↑3.3%)	0.211 (↑2.3%)	0.161 (↑4.3%)	0.191 (↑3.2%)	0.293 (↑3.5%)	0.299 (↑2.7%)	0.257 (↑4.5%)	0.283 (↑3.5%)
	ADJM	0.197 (↑1.3%)	0.208 (↑0.9%)	0.157 (↑1.6%)	0.187 (↑1.2%)	0.287 (↑1.5%)	0.294 (↑1.0%)	0.250 (↑1.8%)	0.277 (↑1.4%)
	TCA	0.198 (↑1.8%)	0.209 (↑1.4%)	0.158 (↑2.3%)	0.188 (↑1.8%)	0.289 (↑1.9%)	0.295 (↑1.5%)	0.251 (↑2.4%)	0.278 (↑1.9%)
	BO	0.196 (↑0.6%)	0.207 (↑0.3%)	0.155 (↑0.7%)	0.186 (↑0.5%)	0.285 (↑0.7%)	0.292 (↑0.5%)	0.247 (↑0.8%)	0.275 (↑0.6%)
	MI-TGAM	<b>0.205 (↑5.4%)</b>	<b>0.215 (↑4.2%)</b>	<b>0.166 (↑7.6%)</b>	<b>0.195 (↑5.6%)</b>	<b>0.297 (↑4.9%)</b>	<b>0.303 (↑4.2%)</b>	<b>0.262 (↑6.8%)</b>	<b>0.287 (↑5.2%)</b>

Table 6: Transfer attack results of MI-TGAM and baseline methods using iTransformer as the surrogate model.

Dataset	Method	Target Model (Using iTransformer as Surrogate Model)							
		MSE (with Degradation Percentage)				MAE (with Degradation Percentage)			
		FrTS	SegRNN	TimesNet	Average	FrTS	SegRNN	TimesNet	Average
ETT	Clean	0.411 (-0.0%)	0.377 (-0.0%)	0.446 (-0.0%)	0.411 (-0.0%)	0.420 (-0.0%)	0.400 (-0.0%)	0.452 (-0.0%)	0.424 (-0.0%)
	FGSM	0.426 (↑3.7%)	0.389 (↑3.4%)	0.451 (↑1.1%)	0.422 (↑2.6%)	0.428 (↑2.1%)	0.408 (↑2.1%)	0.454 (↑0.4%)	0.430 (↑1.5%)
	BIM	0.425 (↑3.6%)	0.389 (↑3.3%)	0.451 (↑1.0%)	0.422 (↑2.6%)	0.428 (↑1.9%)	0.408 (↑2.6%)	0.454 (↑0.3%)	0.430 (↑1.4%)
	PGD	0.422 (↑2.6%)	0.386 (↑2.5%)	0.450 (↑0.7%)	0.419 (↑1.9%)	0.426 (↑1.4%)	0.406 (↑1.4%)	0.453 (↑0.2%)	0.428 (↑1.0%)
	MI-FGSM	0.426 (↑3.7%)	0.390 (↑3.5%)	0.451 (↑1.1%)	0.422 (↑2.7%)	0.428 (↑2.1%)	0.408 (↑2.1%)	0.454 (↑0.4%)	0.430 (↑1.5%)
	ATSG	0.424 (↑3.2%)	0.388 (↑3.1%)	0.450 (↑0.9%)	0.421 (↑2.4%)	0.429 (↑2.1%)	0.409 (↑2.4%)	0.453 (↑0.3%)	0.431 (↑1.5%)
	ADJM	0.411 (↑0.2%)	0.378 (↑0.3%)	0.447 (↑1.0%)	0.412 (↑0.2%)	0.420 (↑0.0%)	0.401 (↑0.4%)	0.452 (↑0.0%)	0.425 (↑0.1%)
	TCA	0.423 (↑2.9%)	0.388 (↑3.0%)	0.450 (↑0.9%)	0.420 (↑2.2%)	0.428 (↑2.0%)	0.409 (↑2.3%)	0.454 (↑0.3%)	0.430 (↑1.5%)
	BO	0.414 (↑0.7%)	0.377 (↑0.1%)	0.450 (↑0.8%)	0.414 (↑0.6%)	0.424 (↑0.9%)	0.401 (↑0.3%)	<b>0.457 (↑1.1%)</b>	0.427 (↑0.8%)
ECL	MI-TGAM	<b>0.439 (↑6.8%)</b>	<b>0.399 (↑5.8%)</b>	<b>0.453 (↑1.5%)</b>	<b>0.430 (↑4.6%)</b>	<b>0.438 (↑4.3%)</b>	<b>0.416 (↑4.0%)</b>	0.455 (↑0.6%)	<b>0.436 (↑2.9%)</b>
Traffic	Clean	0.195 (-0.0%)	0.206 (-0.0%)	0.259 (-0.0%)	0.220 (-0.0%)	0.283 (-0.0%)	0.291 (-0.0%)	0.341 (-0.0%)	0.305 (-0.0%)
	FGSM	0.203 (↑4.0%)	0.212 (↑2.7%)	0.256 (↓1.0%)	0.224 (↑1.6%)	0.293 (↑3.5%)	0.298 (↑2.5%)	0.339 (↓0.8%)	0.310 (↑1.6%)
	BIM	0.199 (↑2.1%)	0.209 (↑1.3%)	0.256 (↓1.0%)	0.221 (↑0.6%)	0.288 (↑1.7%)	0.294 (↑1.1%)	0.338 (↓1.0%)	0.307 (↑0.5%)
	PGD	0.199 (↑2.1%)	0.209 (↑1.2%)	0.256 (↓1.1%)	0.221 (↑0.6%)	0.288 (↑1.7%)	0.294 (↑1.1%)	0.338 (↓1.0%)	0.307 (↑0.5%)
	MI-FGSM	0.202 (↑3.5%)	0.211 (↑2.2%)	0.256 (↓1.0%)	0.223 (↑1.3%)	0.291 (↑2.9%)	0.297 (↑2.0%)	0.338 (↓0.9%)	0.309 (↑1.2%)
	ATSG	0.202 (↑3.8%)	0.212 (↑2.6%)	0.256 (↓1.0%)	0.223 (↑1.6%)	0.294 (↑4.0%)	0.299 (↑3.0%)	0.339 (↓0.7%)	0.311 (↑1.9%)
	ADJM	0.198 (↑1.4%)	0.208 (↑0.9%)	0.256 (↓1.1%)	0.221 (↑0.3%)	0.288 (↑1.6%)	0.294 (↑1.1%)	0.338 (↓0.9%)	0.307 (↑0.5%)
	TCA	0.198 (↑1.8%)	0.209 (↑1.2%)	0.256 (↓1.1%)	0.221 (↑0.5%)	0.288 (↑1.8%)	0.294 (↑1.3%)	0.338 (↓1.0%)	0.307 (↑0.6%)
	BO	0.196 (↑0.6%)	0.207 (↑0.3%)	0.256 (↓1.0%)	0.220 (↓0.1%)	0.285 (↑0.7%)	0.292 (↑0.5%)	0.338 (↓0.9%)	0.305 (↑0.0%)
	MI-TGAM	<b>0.210 (↑7.8%)</b>	<b>0.218 (↑5.6%)</b>	<b>0.259 (↑0.1%)</b>	<b>0.229 (↑4.1%)</b>	<b>0.301 (↑6.4%)</b>	<b>0.305 (↑5.0%)</b>	<b>0.342 (↑0.2%)</b>	<b>0.316 (↑3.6%)</b>

of attack iterations  $K$ , and the input sequence length  $L$  (while keeping the forecast horizon  $H = 96$  fixed). We perform this analysis on the ETT dataset using SegRNN as both the surrogate and target model (white-box setting), with results shown in Fig. 2.

We vary the perturbation budget  $\epsilon$  over the set  $\{0.05, 0.10, 0.15, 0.20\}$ , corresponding to 5%, 10%, 15%, and 20% of the original magnitude. The results show a clear increasing trend where larger budgets lead to higher MSE degradation for all attack methods, as expected. Notably, the performance gap between MI-TGAM and the strongest baselines (PGD and MI-FGSM) widens as  $\epsilon$  increases, demonstrating that MI-TGAM can more effectively exploit larger perturbation budgets to maximize attack effectiveness.

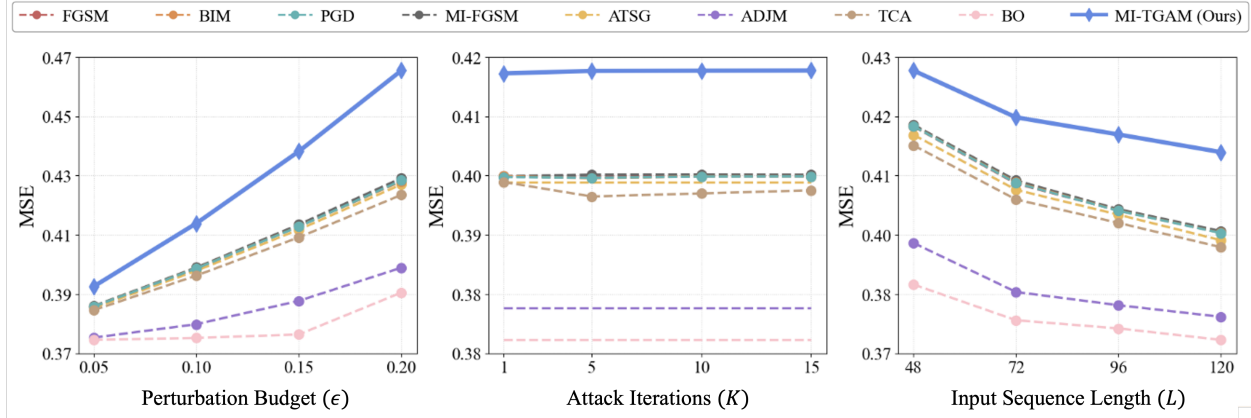


Figure 2: Sensitivity of attack performance (MSE) to key hyperparameters ( $\epsilon$ ,  $K$ , and  $L$ ) on the ETT dataset using SegRNN as the surrogate and target model.

We examine the sensitivity to the number of iterations  $K \in \{1, 5, 10, 15\}$ . MI-TGAM shows consistent advantages over all baselines across all iteration settings. Remarkably, MI-TGAM achieves near-peak attack performance even with a single iteration ( $K = 1$ ), which is equivalent to the TGSM baseline (TGAM without momentum and iteration). This demonstrates the effectiveness of the timestamp-wise gradient accumulation mechanism, which enriches gradient information even in single-step attacks.

Finally, we evaluate the impact of varying the input sequence length  $L \in \{48, 72, 96, 120\}$  while keeping the forecast horizon  $H = 96$  fixed. The results show that all methods exhibit progressively reduced attack effectiveness (lower MSE) as the input sequence length increases. This can be attributed to the fact that longer input sequences generally provide more contextual information, improving the model’s forecasting stability and robustness, thereby increasing the difficulty of successful adversarial attacks. Despite this trend, MI-TGAM consistently outperforms all baseline methods across all input sequence lengths, maintaining a substantial performance advantage even when  $L = 120$ .

In summary, the sensitivity analysis demonstrates the stable and robust performance of MI-TGAM across different hyperparameter settings and task configurations. These results confirm that MI-TGAM is not only effective under the default settings but also maintains its superiority across a wide range of practical scenarios, making it a reliable and versatile attack method for time series forecasting models.

#### 4.5 Visual Analysis

To intuitively understand the effectiveness of MI-TGAM, we visualize adversarial examples and the corresponding model forecasts in Fig. 3. These visualizations are derived from a randomly selected sample and a specific variable on the Electricity dataset, comparing MI-TGAM against baseline methods using SegRNN as both the surrogate and target model (white-box setting), with perturbation budgets  $\epsilon \in \{0.05, 0.10, 0.15, 0.20\}$ .

From the left subfigures of Fig. 3, we observe that despite the increasing perturbation budget, the adversarial examples generated by MI-TGAM maintain high visual similarity to the original input in terms of overall trend and temporal patterns. Unlike baseline methods that often introduce high-frequency, chaotic noise that is easily detectable, MI-TGAM produces perturbations with a more regular and smooth pattern that preserves the natural characteristics of time series data. This makes MI-TGAM’s perturbations more stealthy and harder to detect, which is crucial for practical adversarial attacks.

As shown in the right subfigures of Fig. 3, the forecasting results demonstrate that MI-TGAM does not merely introduce random variance in the predictions like other baseline methods. Instead, MI-TGAM induces significant deviations from the ground truth. Specifically, we observe that MI-TGAM amplifies prediction errors in critical regions such as peaks, valleys, and high-volatility areas, where accurate forecasting is most important. This targeted error amplification directly enhances the adversarial effect, making MI-TGAM particularly effective at degrading the practical utility of forecasting models. In contrast, baseline methods produce more scattered errors that are less impactful on the overall forecasting quality.

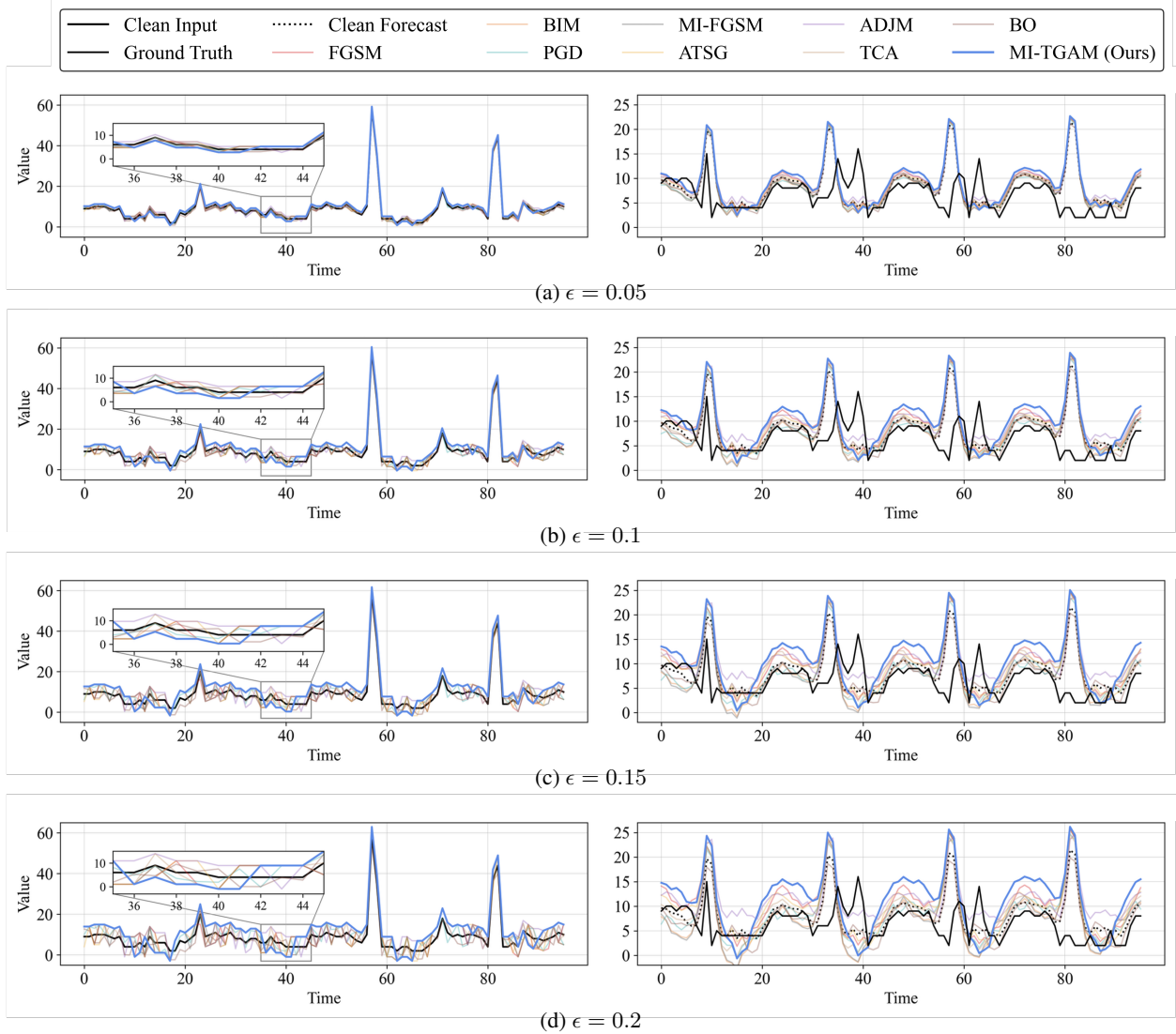


Figure 3: Visualization of the adversary conducted by all methods using SegRNN as the surrogate and the target model on ECL dataset with varying perturbation budgets  $\epsilon$ . The left panels show the clean and perturbed input samples, the right panels show the corresponding forecasting outputs.

Overall, these visualizations confirm that MI-TGAM generates adversarial examples that are both effective (causing significant prediction errors) and stealthy (maintaining natural appearance), making it a powerful and practical attack method for time series forecasting models.

#### 4.6 Comparison in Temporal Inconsistent Settings

To further verify attack performance of proposed MI-TGAM, we compare it with all baseline methods in temporal inconsistent settings. Unlike the former settings, here we relax the TUAP constraint, allowing the same time stamp across different samples could have different perturbations. The experiment is conducted on the Traffic dataset in both white-box attack and transfer attack scenarios using TimesNet as the surrogate model. The results are shown in Table 7.

In the white-box attack, the attack strength of MI-TGAM is lower than that of unconstrained baseline methods, which is as expected. This disparity arises because temporal inconsistent methods possess a significantly larger optimization space, allowing them to exploit per-window gradients independently without adhering to temporal constraints. The results empirically show that imposing a strict temporal-consistency constraint necessitates a trade-off in local optimization potency.

Table 7: The white-box attack and transfer attack results of MI-TGAM and baseline methods using TimesNet as the surrogate model on Traffic dataset in temporal inconsistent setting. White-box attack results are presented in gray.

Method	Degradation Percentage on MSE				
	TimesNet	FreTS	SegRNN	iTransformer	Average
FGSM	85.88%	1.49%	-3.03%	2.04%	0.17%
BIM	85.88%	1.49%	-3.03%	2.04%	0.17%
PGD	59.57%	1.06%	-3.31%	1.47%	-0.26%
MI-FGSM	85.88%	1.49%	-3.03%	2.04%	0.17%
ATSG	103.66%	1.09%	-3.03%	1.53%	-0.14%
ADJM	<b>105.25%</b>	0.31%	-3.49%	0.52%	-0.89%
TCA	103.66%	1.09%	-3.03%	1.53%	-0.14%
BO	0.38%	0.28%	-3.70%	0.42%	-1.00%
MI-TGAM	15.48%	<b>2.18%</b>	<b>-2.69%</b>	<b>3.12%</b>	<b>0.87%</b>

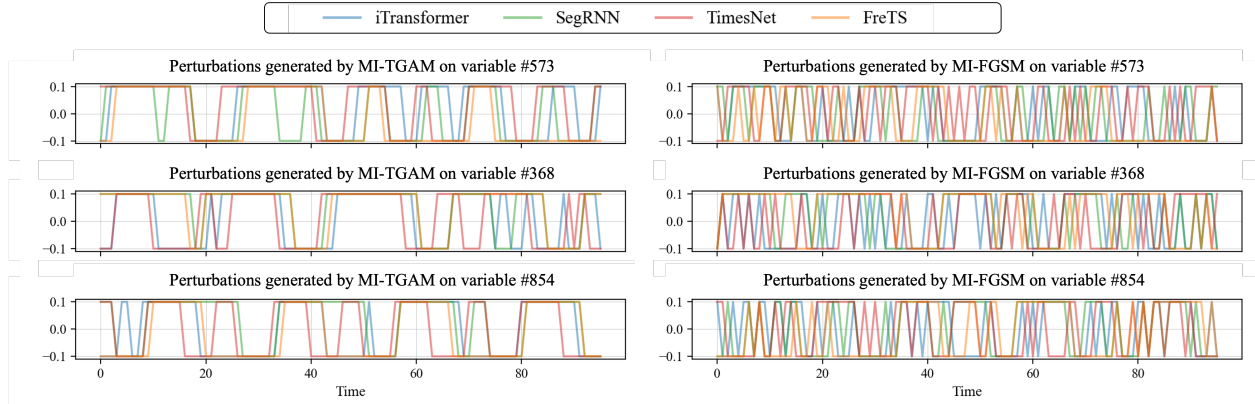


Figure 4: Perturbations generated by MI-TGAM (left) and MI-FGSM (right) under four surrogate models with three randomly selected variable within a randomly selected sample on Traffic dataset.

Despite the deficit in white-box attack, MI-TGAM demonstrates superior performance in cross-model transfer attacks, consistently achieving the highest transfer attack results. These findings suggest that, compared to unconstrained baseline methods, MI-TGAM can enhance the attack strength in transfer attacks under temporal inconsistent settings.

To elucidate the underlying mechanism driving the high transferability of MI-TGAM, we visualize the perturbations generated by MI-TGAM and MI-FGSM across three randomly selected variable within a randomly selected sample on Traffic dataset in Fig. 4.

Comparing the perturbations on different surrogate models, the perturbations generated by MI-TGAM (left column) exhibit a high degree of consistency in the perturbation trajectory. In contrast, the perturbations generated by MI-FGSM (right column) are chaotic and divergent, with significant differences between the different surrogate models. These results indicate that MI-TGAM successfully extracts robust vulnerability patterns that are shared across different neural architectures.

## 5 Conclusion

This paper aims to address the critical yet overlooked issue of temporal inconsistency in adversarial attacks on time series forecasting. To this end, we introduce the concept of Temporally Unified Adversarial Perturbations (TUAPs), propose the Timestamp-wise Gradient Accumulation Method (TGAM), and further incorporate TGAM into a momentum-based iterative framework (MI-TGAM). Comprehensive experiments on benchmark datasets and diverse model architectures demonstrate the effectiveness and superiority of our proposed method. In the future, we will extend TUAPs into attacking time series classification models and establishing a robust defense mechanism against such temporally consistent attacks.

## References

[1] Sheraz Aslam, Herodotos Herodotou, Syed Muhammad Mohsin, Nadeem Javaid, Nouman Ashraf, and Shahzad Aslam. A survey on deep learning methods for power load and renewable energy forecasting in smart microgrids.

*Renewable and Sustainable Energy Reviews*, 144:110992, 2021. ISSN 1364-0321. doi: 10.1016/j.rser.2021.110992. URL <https://www.sciencedirect.com/science/article/pii/S1364032121002847>.

- [2] Bo Xu, Zhiqiang Liu, Haolin Zhu, Bingqing Dong, Bo Zhao, Ben Yan, and Jun Wei. A Novel Adversarial Attack Method for Time-Series Regression Models in IIoT-Based Digital Twins. *IEEE Internet of Things Journal*, 12(15):29278–29290, 2025. ISSN 2327-4662. doi: 10.1109/JIOT.2025.3569857. URL <https://ieeexplore.ieee.org/abstract/document/11004038>.
- [3] Kenniy Olorunnimbe and Herna Viktor. Deep learning in the stock market—a systematic survey of practice, backtesting, and applications. *Artificial Intelligence Review*, 56(3):2057–2109, 2023. ISSN 1573-7462. doi: 10.1007/s10462-022-10226-0. URL <https://doi.org/10.1007/s10462-022-10226-0>.
- [4] Christian Szegedy, Wojciech Zaremba, Ilya Sutskever, Joan Bruna, Dumitru Erhan, Ian Goodfellow, and Rob Fergus. Intriguing properties of neural networks, 2014. URL <http://arxiv.org/abs/1312.6199>.
- [5] Ian J. Goodfellow, Jonathon Shlens, and Christian Szegedy. Explaining and Harnessing Adversarial Examples, 2015. URL <http://arxiv.org/abs/1412.6572>.
- [6] Gautam Raj Mode and Khaza Anuarul Hoque. Adversarial Examples in Deep Learning for Multivariate Time Series Regression. In *2020 IEEE Applied Imagery Pattern Recognition Workshop (AIPR)*, pages 1–10, 2020. doi: 10.1109/AIPR50011.2020.9425190. URL <https://ieeexplore.ieee.org/abstract/document/9425190>.
- [7] René Heinrich, Christoph Scholz, Stephan Vogt, and Malte Lehna. Targeted adversarial attacks on wind power forecasts. *Machine Learning*, 113(2):863–889, 2024. ISSN 1573-0565. doi: 10.1007/s10994-023-06396-9. URL <https://doi.org/10.1007/s10994-023-06396-9>.
- [8] Taha Belkhouja, Yan Yan, and Janardhan Rao Doppa. Dynamic Time Warping Based Adversarial Framework for Time-Series Domain. *IEEE Transactions on Pattern Analysis and Machine Intelligence*, 45(6):7353–7366, 2023. ISSN 1939-3539. doi: 10.1109/TPAMI.2022.3224754. URL <https://ieeexplore.ieee.org/abstract/document/9970291>.
- [9] Tao Wu, Xuechun Wang, Shaojie Qiao, Xingping Xian, Yanbing Liu, and Liang Zhang. Small perturbations are enough: Adversarial attacks on time series prediction. *Information Sciences*, 587:794–812, 2022. ISSN 0020-0255. doi: 10.1016/j.ins.2021.11.007. URL <https://www.sciencedirect.com/science/article/pii/S0020025521011178>.
- [10] Ziyu Shen and Yun Li. Temporal characteristics-based adversarial attacks on time series forecasting. *Expert Systems with Applications*, 264:125950, 2025. ISSN 0957-4174. doi: 10.1016/j.eswa.2024.125950. URL <https://www.sciencedirect.com/science/article/pii/S0957417424028173>.
- [11] Runhai Jiao, Zhuoting Han, Xuan Liu, Changyu Zhou, and Min Du. A Gradient-Based Wind Power Forecasting Attack Method Considering Point and Direction Selection. *IEEE Transactions on Smart Grid*, 15(3):3178–3192, 2024. ISSN 1949-3061. doi: 10.1109/TSG.2023.3325390. URL <https://ieeexplore.ieee.org/abstract/document/10304287>.
- [12] Haixu Wu, Tengge Hu, Yong Liu, Hang Zhou, Jianmin Wang, and Mingsheng Long. TimesNet: Temporal 2d-variation modeling for general time series analysis. In *The Eleventh International Conference on Learning Representations*, 2022. URL [https://openreview.net/forum?id=ju\\_Uqw384Oq](https://openreview.net/forum?id=ju_Uqw384Oq).
- [13] Yong Liu, Tengge Hu, Haoran Zhang, Haixu Wu, Shiyu Wang, Lintao Ma, and Mingsheng Long. iTransformer: Inverted transformers are effective for time series forecasting. In *The Twelfth International Conference on Learning Representations*, 2023. URL <https://openreview.net/forum?id=JePfAI8fah>.
- [14] Daizong Ding, Mi Zhang, Fuli Feng, Yuanmin Huang, Erling Jiang, and Min Yang. Black-Box Adversarial Attack on Time Series Classification. *Proceedings of the AAAI Conference on Artificial Intelligence*, 37(6):7358–7368, June 2023. ISSN 2374-3468. doi: 10.1609/aaai.v37i6.25896.
- [15] Gautam Raj Mode and Khaza Anuarul Hoque. Adversarial Examples in Deep Learning for Multivariate Time Series Regression. In *2020 IEEE Applied Imagery Pattern Recognition Workshop (AIPR)*, pages 1–10, October 2020. doi: 10.1109/AIPR50011.2020.9425190.
- [16] Alexey Kurakin, Ian Goodfellow, and Samy Bengio. Adversarial examples in the physical world, 2017. URL <http://arxiv.org/abs/1607.02533>.
- [17] Aleksander Madry, Aleksandar Makelov, Ludwig Schmidt, Dimitris Tsipras, and Adrian Vladu. Towards Deep Learning Models Resistant to Adversarial Attacks, 2019. URL <http://arxiv.org/abs/1706.06083>.
- [18] Yinpeng Dong, Fangzhou Liao, Tianyu Pang, Hang Su, Jun Zhu, Xiaolin Hu, and Jianguo Li. Boosting Adversarial Attacks with Momentum, 2018. URL <http://arxiv.org/abs/1710.06081>.
- [19] Jiadong Lin, Chuanbiao Song, Kun He, Liwei Wang, and John E. Hopcroft. Nesterov Accelerated Gradient and Scale Invariance for Adversarial Attacks. In *International Conference on Learning Representations*, September 2019.

- [20] Xiaosen Wang and Kun He. Enhancing the Transferability of Adversarial Attacks Through Variance Tuning. In *Proceedings of the IEEE/CVF Conference on Computer Vision and Pattern Recognition*, pages 1924–1933, 2021.
- [21] Yanpei Liu, Xinyun Chen, Chang Liu, and Dawn Song. Delving into Transferable Adversarial Examples and Black-box Attacks. In *International Conference on Learning Representations*, February 2017.
- [22] Cihang Xie, Zhishuai Zhang, Yuyin Zhou, Song Bai, Jianyu Wang, Zhou Ren, and Alan L. Yuille. Improving Transferability of Adversarial Examples With Input Diversity. In *Proceedings of the IEEE/CVF Conference on Computer Vision and Pattern Recognition*, pages 2730–2739, 2019.
- [23] Yinpeng Dong, Tianyu Pang, Hang Su, and Jun Zhu. Evading Defenses to Transferable Adversarial Examples by Translation-Invariant Attacks. In *Proceedings of the IEEE/CVF Conference on Computer Vision and Pattern Recognition*, pages 4312–4321, 2019.
- [24] Qihan Wang, Jiaqi Ruan, Xiangrui Meng, Yifan Zhu, Gaoqi Liang, and Junhua Zhao. Investigation of Artificial Intelligence Vulnerability in Smart Grids: A Case from Solar Energy Forecasting. In *2023 IEEE 7th Conference on Energy Internet and Energy System Integration (EI2)*, pages 5207–5212, December 2023. doi: 10.1109/EI259745.2023.10512845. URL <https://ieeexplore.ieee.org/document/10512845>.
- [25] Shuhuai Ren, Yihe Deng, Kun He, and Wanxiang Che. Generating Natural Language Adversarial Examples through Probability Weighted Word Saliency. In Anna Korhonen, David Traum, and Lluís Màrquez, editors, *Proceedings of the 57th Annual Meeting of the Association for Computational Linguistics*, pages 1085–1097, Florence, Italy, July 2019. Association for Computational Linguistics. doi: 10.18653/v1/P19-1103.
- [26] Xinze Zhang, Junzhe Zhang, Zhenhua Chen, and Kun He. Crafting Adversarial Examples for Neural Machine Translation. In Chengqing Zong, Fei Xia, Wenjie Li, and Roberto Navigli, editors, *Proceedings of the 59th Annual Meeting of the Association for Computational Linguistics and the 11th International Joint Conference on Natural Language Processing (Volume 1: Long Papers)*, pages 1967–1977, Online, August 2021. Association for Computational Linguistics. doi: 10.18653/v1/2021.acl-long.153.
- [27] Kun Yi, Qi Zhang, Wei Fan, Shoujin Wang, Pengyang Wang, Hui He, Ning An, Defu Lian, Longbing Cao, and Zhendong Niu. Frequency-domain MLPs are More Effective Learners in Time Series Forecasting. *Advances in Neural Information Processing Systems*, 36:76656–76679, December 2023. URL [https://proceedings.neurips.cc/paper\\_files/paper/2023/hash/f1d16af76939f476b5f040fd1398c0a3-Abstract-Conference.html](https://proceedings.neurips.cc/paper_files/paper/2023/hash/f1d16af76939f476b5f040fd1398c0a3-Abstract-Conference.html).
- [28] Shengsheng Lin, Weiwei Lin, Wentai Wu, Feiyu Zhao, Ruichao Mo, and Haotong Zhang. SegRNN: Segment Recurrent Neural Network for Long-Term Time Series Forecasting, 2023. URL <http://arxiv.org/abs/2308.11200>.